Advanced Control Functionalities for Grid Integration of Large Scale Wind Generation

Fernanda Resende, Rogério Almeida, Ângelo Mendonça and João Peças Lopes

Abstract Many system operators have issued grid code requirements to ensure a reliable and secure operation of power systems with high integration levels of wind generation. Then, wind farms are required to behave as much as possible like conventional power plants equipped with synchronous generators, providing thus active and reactive power regulation and fault ride through capability. In addition, it is necessary to assure that problems of small signal stability do not arise. This chapter deals with advanced control functionalities to improve the performance of double fed induction generators, regarding frequency control and fault ride through capability, and with robust tuning of classical power system stabilizers installed in double fed induction generators to provide damping as an ancillary service. Since fault ride through is a matter of major concern for many system operators, the control functionalities of a static compensator based solution to provide fault ride through capability of wind farms equipped with fixed speed induction generators are also addressed. The effectiveness of the above mentioned advanced control functionalities is demonstrated through numerical simulations.

F. Resende (✉) · R. Almeida · Â. Mendonça · J. P. Lopes
INESC-Porto, Porto, Portugal
e-mail: fresende@inescporto.pt

J. P. Lopes
Faculty of Engineering of Porto University, Porto, Portugal

R. Almeida
Federal University of Amapá, Amapá, Brazil

F. Resende
Lusófona University of Porto, Porto, Portugal

P. M. Pardalos et al. (eds.), *Handbook of Wind Power Systems*, Energy Systems,
DOI: 10.1007/978-3-642-41080-2_9,

1 Introduction

The widespread growth of wind power capacity installed worldwide required the development of larger and more robust Wind Turbine Generation Systems (WTGS). Requirements in terms of power control ability during normal operation and in case of grid abnormalities have increased significantly, leading with the variable speed concept with Double Fed Induction Generator (DFIG) systems and with WTGS equipped with full-scale power converters. In the DFIG configuration, only the rotor of the induction generator is connected to the ac grid through a partial-scale frequency converter, which is responsible to control the rotor speed in order to allow a wide speed range of operation. Typically, the variable speed range is ± 30 % around the synchronous speed and the frequency converter rating is only 25–30 % of the configuration rated power, which makes this concept attractive and popular for an economic view point [29]. As a result the DFIG has been the most commonly used generator type [18].

Following the increasing wind power integration levels, many system operators have updated their grid codes, through the establishment of specific and stricter technical requirements for wind farms operation [15]. In many systems, wind generation has priority over conventional power plants usually equipped with synchronous generators, which could not be dispatched in order to accommodate the surplus of wind generation. As a result, several negative impacts can arise regarding the system technical and operational characteristics, focusing particularly on the reduction of system dynamic stability and security of supply and on system frequency and voltage regulation capabilities. Therefore, the most common grid code requirements focus mainly the control ability of wind farms regarding both active and reactive power control to provide frequency and voltage regulation, respectively, and Fault Ride-Through (FRT) capability [54].

Synchronous generators may be equipped with Power System Stabilizers (PSS) in order to provide damping to low frequency power oscillations occurring among their rotors. As the large surplus of wind generation in some areas may increase the power flows between weakly interconnected grids, the damping levels will be reduced since the existing PSS may no longer be able to provide the additional damping necessary in all wind generation conditions [33]. Therefore, wind farms should be able to supply damping as an ancillary service [23, 24].

Grid code requirements have been the major drivers for the fast developments of WTGS Wind turbine generation systems—WTGS technologies over the past few years [20]. Their compliance has challenged the manufacturers to develop conventional control capabilities for wind turbines and therefore for wind farms, exploiting the variable speed concept. For this purpose, advanced control functionalities have been developed and embedded into the control systems of the individual WTGS frequency converters, providing thus enlarged control capabilities, which play a key role to support the most stringent grid code requirements issued by many system operators.

Requirements in terms of active and reactive power control, under normal operating conditions, have been addressed through an hierarchical control structure comprising both a central control level and a local control level supported by an advanced SCADA system [4, 20]. Depending on the network status, the system operator may require adjustments in outputs of active and reactive power of the wind farm. For this purpose a two level hierarchical control and management system has been exploited. The central control level is responsible to control the wind farm output power by sending out active and reactive power references to the local control level. The main parameters from the individual WTGS and from the Point of Common Coupling (PCC) are recorded by the data acquisition system and used to determine the optimum active and reactive power set points for each WTGS in order to meet the system operator requests. The local control level addresses the control system of individual WTGS and ensures that the references sent from the wind farm central control level are achieved.

FRT capability has been the major concern of network operators since the effects of grid faults may propagate over very large geographical areas leading with the disconnection of wind farms. Therefore a serious threat will be created regarding the network security of supply because a large amount of wind generation could be lost simultaneously. In order to prevent this problem WTGS must remain connected during and after severe grid disturbances, ensuring fast restoration of active power to pre-fault levels as soon as the fault is cleared and injecting reactive current in order to support the grid voltage during disturbances, providing thus fast voltage recovery after fault clearing.

In spite of the current use of variable speed WTGS, many wind farms equipped with Fixed Speed Induction Generators (FSIG), the standard technology installed in the early 1990s, are still in operation in many countries and can fulfil FRT requirements to a different degree. The dynamic behaviour of FSIG is dominated by the grid connected induction generator which always draws reactive power from the grid. Although shunt capacitor batteries are typically used to compensate the reactive power requirements during steady state operation, these devices exhibit rather poor performance during fault conditions, since their reactive power injection capability decreases significantly during voltage drops. Thus, in the event of voltage dip the generator torque and active power output can be reduced considerably resulting in rotor acceleration and further rotor instability. Also, the machine operation at increased slip values results in increased reactive power absorption, particularly after fault clearance and partial restoration of the system voltage. This effectively prevents voltage recovery and may affect other neighbouring generators whose terminal voltage remains depressed. Since the dynamic behaviour of the induction generator itself can not be improved, FRT capability can be assisted by external static compensation devices connected at the wind farm terminals [46]. For this purpose, STATic synchronous COMpensator (STATCOM) based solutions are considered the most effective approaches for these situations [11]. However, a STATCOM rating approximately 100 % of the total wind farm installed capacity is required to guarantee a successful voltage recovery [8, 19, 36, 46].

This chapter deals with the advanced control functionalities, which have been developed to enhance the performance of DFIG control capabilities regarding the compliance with grid code requirements, particularly FRT capability and primary frequency control. The problem of PSS robustly tuning in systems with large share of wind generation is also addressed in this chapter, taking into account that PSS installed in DFIG can be used to provide additional damping to the electromechanical modes of oscillation. Moreover, the control functions of an external STATCOM based solution to provide FRT capability of wind farms equipped with FSIG are also addressed. The performance of these advanced control functionalities as well as the performance of the robustly tuned PSS is evaluated through numerical simulations performed in small test systems. The results obtained are presented and discussed.

In Sect. 2 the mathematical model of the DFIG configuration is presented together with the main issues regarding DFIG operation and control; Sect. 3 describes control functions based on fuzzy control that can be used to improve FRT capability of DFIG; Sect. 4 presents a robust primary frequency control approach for DFIG; A suitable approach to perform robust tuning of PSS installed in DFIG is addressed in Sect. 5; Sect. 6 deals with the commonly used control approaches of STATCOM when used to provide FRT capability of wind farms equipped with FSIG. Final remarks are presented in Sect. 7.

2 DFIG Dynamic Modelling and Operation

The DFIG concept corresponds to a variable speed WTGS equipped with a Wound Rotor Induction Generator (WRIG) and a partial scale frequency converter connected to the rotor windings through slip rings. The stator is directly connected to the ac grid whereas the rotor is connected through the frequency converter, being the DFIG fed from both the rotor and stator sides, as it can be observed from the typical electrical scheme depicted in Fig. 1. Thus, the DFIG configuration allows supplying electrical power to the grid from the stator and exchanging electrical power with the grid through the rotor circuit. Also, controlling the active power flow on the rotor circuit, both in magnitude and direction, allows the variable speed operation feature over a wide speed range, from sub synchronous to super synchronous speed. Therefore, the frequency converter comprises two Insulate Gate Bipolar Transistors (IGBT) based Pulse Width Modulation (PWM) converters, the Rotor Side Converter (RSC) and the Grid Side Converter (GSC), connected back-to-back through a dc-link capacitor and controlled independently of each other [40, 44], as it can be observed from Fig. 1.

During normal operating conditions, the RSC control system is responsible to control the active and reactive power fed into the grid though the stator circuit by controlling the rotor current components while the GSC control system is responsible to control the dc-link voltage based on the active power balance between the RSC and the ac grid and, additionally, to ensure the DFIG operation

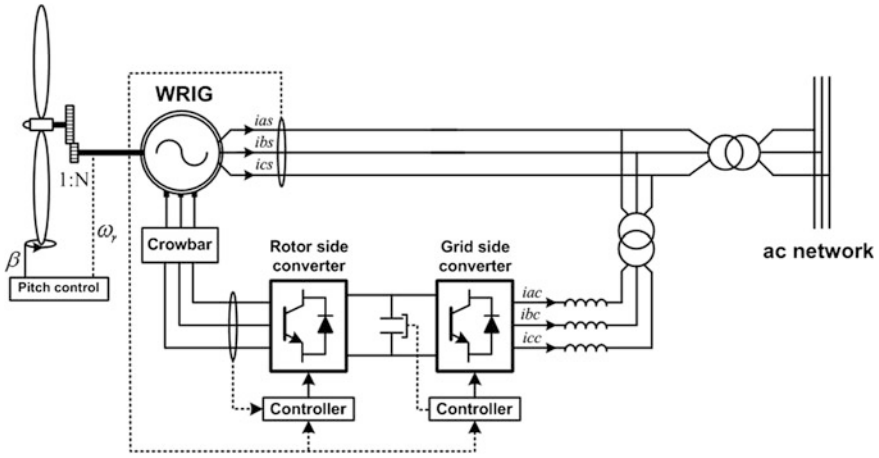

Fig. 1 Typical configuration of the DFIG electrical part

with a given power factor. However, since the RSC can compensate a bigger reactive power demand than the GSC, it is usually assumed that the reactive power demand is mainly controlled by means of the RSC [1, 7, 34].

In case of a grid fault, high transient currents arise in the grid connected WRIG stator, which are transferred to the rotor leading to over currents and over voltages that can damage the frequency converter. In order to avoid these over currents an ac crowbar protection system has been commonly used, being triggered by the dc-link voltage, which rises rapidly due to the rotor current peaks. Then, for dip voltage sags, the crowbar short-circuits the WRIG rotor and the DFIG configuration goes temporarily to an asynchronous machine operation mode, since RSC is blocked and the WRIG controllability is lost. In contrast to the RSC, the GSC is kept in operation. So, in order to provide voltage support under these circumstances, a co-ordinated voltage control of RSC and GSC is required. Thus, in the adopted control strategy, as long as the crowbar is triggered, the GSC will provide its maximum reactive power in order to improve the voltage level. When the crowbar is removed, the RSC is taking over the voltage control in order to re-establish immediately the voltage level. In this way the DFIG configuration will be able to comply with the requirements of FRT and grid support capability [1, 34].

The mathematical models commonly used to represent the DFIG dynamic behaviour with impact on the ac network during transient stability studies share a high degree of complexity. A generic model is based on the typical DFIG configuration illustrated in Fig. 1, comprising basically the following main components:

- The aerodynamic system;
- The mechanical system;
- The generator (WRIG);

- The frequency converter and the corresponding control systems;
- The pitch control system.

Suitable dynamic models for these main components and their interconnections are presented in the following sections. These models are intended for power stability studies. Therefore, the control functionalities of the frequency converter are addressed under the framework of the control systems of both RSC and GSC [13, 17, 31, 41].

2.1 The Aerodynamic System

The WTGS aerodynamic system, also called the wind turbine rotor, comprises the turbine blades, which are responsible for reducing the incoming wind speed and for transforming the absorbed kinetic energy into mechanical power. The basic physics related with this energy conversion as well as with the mathematical representation of the turbine rotor are reported in [1, 2].

The amount of the kinetic energy extracted from the incoming wind in the turbine rotor swept area will depend on the wind turbine efficiency usually known as power coefficient, C_p. In turn, the C_p will depend on the angle of attack between the plane of the moving rotor blades and the relative wind speed as seen from the moving blades. Thus, the angle of attack is typically expressed in term of the tip speed ratio, λ, commonly defined as the relationship between the blade tip linear speed and the incoming wind speed as

$$\lambda = \frac{\omega_{turb} R}{V_w}, \tag{1}$$

where ω_{turb}(rad-elec/s) is the wind turbine rotor speed, V_w(m/s) is the incoming wind speed and R(m) is the blade radius.

In pitch controlled wind turbines, the angle of attack can be modified according to the pitch angle of the blades, β, which is adjusted through the pitch control system. Therefore, the power coefficient is commonly expressed as a function of λ and β, $C_p(\lambda, \beta)$.

Then, from a physical point of view, the wind turbine rotor is typically represented through the relationship between the available wind power, P_{wind}, and the mechanical power output, P_m, as

$$P_m = C_p(\lambda, \beta)\, P_{wind} = \frac{1}{2} \rho C_p(\lambda, \beta) A V_w^3, \tag{2}$$

where P_m(W) is the mechanical power on the turbine shaft, A(m^2) is the swept area by the turbine blades and $\rho = 1{,}225$ (kg/m^3) is the air density.

Numerical approximations have been developed to calculate C_p as a function of both λ and β. The following approximation was adopted as suggested by [51].

$$C_p(\lambda,\beta) = 0.73\left(\frac{151}{\lambda_i} - 0.58\beta - 0.002\beta^{2.14} - 13.2\right)e^{-18.4/\lambda_i} \tag{3}$$

where

$$\lambda_i = \frac{1}{\frac{1}{\lambda - 0.02\beta} - \frac{0.003}{\beta^3+1}} \tag{4}$$

Equations (3) and (4) lead to the $C_p(\lambda,\beta)$ versus λ characteristic curves for several values of the pitch angle of the blades, β (in degrees), and can be used for different wind turbines since the difference between the corresponding power curves can be neglected in dynamic simulation studies as demonstrated in [51]. Thus, the mathematical representation of the wind turbine rotor is commonly approached by a C_p–λ–β characteristic implemented through a look up table. The link between the aerodynamic and mechanical systems will be either mechanical power or mechanical torque, T_m. They are related to each other through the wind turbine rotational speed, ω_{turb}(mec-rad/s), as $P_m = \omega_{turb}T_m$.

2.2 The Mechanical System

The wind turbine mechanical system consists of the drive train comprising the rotating masses, the gear box and the connecting shafts. Thus, the drive train is commonly represented through the corresponding inertia of the system.

The major sources of inertia lie in both the turbine and WRIG rotors. Since the tooth wheels of the gearbox contribute only with a small fraction, the gear inertia is often neglected and only the transformation ratio is included. Thus, a typical model for the mechanical system is a two-mass model with a connecting shaft [50]. However, due to the decoupling effect of the power electronic converters of variable speed WTGS, the shaft properties are hardly reflected at the ac network, as discussed in [51]. Thus, it was assumed that the wind turbine rotor is modelled as a lumped mass only, leading to a more damped behaviour than when a two-mass model is used [50]. Therefore, the effects of torsional oscillations and stress on the turbine shaft were not considered. Such an assumption, however, does not compromise the quality of the comparative analysis regarding the advanced control functionalities to be addressed, as stated in [5–7].

2.3 The Wound Rotor Induction Generator

Representing the WRIG by a simple voltage behind a transient reactance equivalent circuit is a conventional modelling technique in wind turbine based DFIG applications for system dynamic behaviour analysis. The WRIG can be regarded

as a conventional induction generator with a nonzero rotor voltage and represented by a reduced order model, neglecting the dc component and the fast transients in the stator current. In addition, the WRIG is operated as a generator and it is considered that the stator currents are positive when flowing towards the network, as it can be observed from Fig. 1, and the active and reactive power are positive when fed into the grid.

The equations describing the WRIG dynamics are derived with the rotor variables referred to the stator and transformed into the synchronous d–q axis reference frame with the q-axis 90° ahead the d-axis in the direction of the rotation flux. According to [7, 13, 26], the electrical equations of the WRIG rotor can be written in per unit as follows:

$$\begin{cases} \frac{de_d}{dt} = -\frac{1}{T_0}\left[e_d - (X - X')i_{qs}\right] + s\omega_s e_q - \omega_s \frac{L_m}{L_{rr}} \upsilon_{qr} \\ \frac{de_q}{dt} = -\frac{1}{T_0}\left[e_q - (X - X')i_{qs}\right] - s\omega_s e_d + \omega_s \frac{L_m}{L_{rr}} \upsilon_{dr} \end{cases}, \tag{5}$$

where

- e_d and e_q are, respectively, the per unit direct and quadrature components of the voltage behind the transient reactance;
- i_{ds} and i_{qs} are, respectively, the per unit direct and quadrature components of the stator current;
- υ_{dr} and υ_{qr} are, respectively, the per unit direct and quadrature components of the rotor voltage;
- T_0 is the rotor open circuit time constant in seconds;
- X is the per unit open circuit reactance;
- X' is the per unit short circuit reactance;
- L_m is the per unit mutual magnetizing inductance between the stator and the rotor windings;
- L_{rr} is the per unit self-inductance of the rotor windings;
- ω_s is the rotational speed of the synchronous reference frame in rad/s;
- $s\omega_s = (\omega_s - \omega_r)$ is the slip frequency;
- s is the slip;
- ω_r is the generator rotor speed in rad/s;

To complete the WRIG model the differential equations given by (5) have to be combined with the rotor swing equation that provides the rotor speed state variable as

$$\frac{d\omega_r}{dt} = \frac{1}{J}(T_m - T_e - D\omega_r), \tag{6}$$

where T_m is the mechanical torque, T_e is the electromechanical torque, J is the total moment of inertia (kg m^2) accounting both the turbine and the generator rotor inertia and D is the damping factor.

According to [7], the electromagnetic torque can be calculated as

$$T_e = e_d i_{ds} + e_q i_{qs} \tag{7}$$

where i_{ds} and i_{qs} can be derived algebraically from the stator voltage equations given by (8).

$$\begin{cases} \upsilon_{ds} = -R_s i_{ds} + X' i_{qs} + e_d \\ \upsilon_{qs} = -R_s i_{qs} - X' i_{ds} + e_q \end{cases}, \tag{8}$$

The active and reactive power in both stator and the rotor can be calculated as

$$\begin{cases} P_s = T_e \omega_r = \upsilon_{ds} i_{ds} + \upsilon_{qs} i_{qs} \\ Q_s = \upsilon_{qs} i_{ds} - \upsilon_{ds} i_{qs} \end{cases} \tag{9}$$

$$\begin{cases} P_r = -sP_s = \upsilon_{dr} i_{dr} + \upsilon_{qr} i_{qr} \\ Q_r = \upsilon_{qr} i_{dr} - \upsilon_{dr} i_{qr} \end{cases} \tag{10}$$

The active power delivered to the grid is then

$$P_g = P_s + P_r \tag{11}$$

In turn, the mechanical power can be obtained as

$$P_m = \omega_r T_m = (1 - s) P_s \tag{12}$$

It is assumed that T_m, T_e and P_m are positive values for generation. Thus, during sub-synchronous operation $s > 0$, $P_r < 0$, $P_m < P_s$ and so the rotor absorbs power from the stator. On the other hand, during the super-synchronous operation, $s < 0$, $P_r > 0$, $P_m > P_s$ and the rotor produces power, being the power delivered to the grid through both the stator and rotor circuits.

2.4 The DFIG Control Scheme

The variable speed feature makes it possible to adjust the turbine rotational speed to its optimum value, thus maximizing the power coefficient and, therefore, the generated power for several wind speeds below the rated wind. The power speed wind turbine characteristic obtained from Eq. (2) has been commonly used for tracking the WRIG rotor speed to the optimum tip speed ratio, λ_{opt}. According to [4], the speed control aims to keep the DFIG operation according to the pre-defined maximum power extraction curve defined as:

$$P_{ref} = k_{opt} \omega_r^3, \tag{13}$$

where

$$k_{opt} = \frac{1}{2} \rho \frac{C_{p\,opt}}{\lambda_{\text{opt}}^3} \pi R^5 \tag{14}$$

and

$$\omega_{r\,ref} = \frac{p}{2} G \omega_{turb\,opt} \tag{15}$$

is the rotor speed of the generator, being p the number of poles of the WRIG and G the gearbox transmission ratio. Thus, the optimal speed of the turbine shaft can be derived from the Eq. (1) and be rewritten as:

$$\omega_{turb\,opt} = \frac{\lambda_{opt} V_w}{R}, \tag{16}$$

where the value of λ_{opt} can be obtained from the roots of the derivative of Eq. (3) regarding the tip speed ratio.

The DFIG whole control scheme comprises two main control systems: The mechanical control of the wind turbine pitch angle and the electrical control on the frequency converter. Thus, in order to control the power balance and thereby also the rotational speed, some coordination between these two control systems is required. During partial load conditions the electrical control assures variable speed operation while the pitch angle of the blades is kept constant. Above the rated wind speed the pitch angle is increased in order to decrease the power coefficient and, therefore, to shed some of the aerodynamic power, being the wind turbine shaft speed controlled to its rated value and therefore the DFIG output is kept near its rated power.

The frequency converter control scheme has been commonly designed to regulate the rotor speed of the WRIG in order to track the optimal wind speed reference, $\omega_{turb\,opt}$, for maximum power extraction given the incoming wind speed. For this purpose, the electrical control scheme is based on the WRIG rotor current regulation on the stator flux oriented reference frame, in which the d-axis is aligned with the stator flux linkage axis, being the quadrature component of the stator voltage, υ_{qs}, equal to the terminal voltage, V_s, and the direct component of the stator voltage υ_{ds} equal to zero [28, 38]. This yields the following equations regarding the stator currents:

$$\begin{cases} i_{ds} = -\frac{1}{L_{ss}} \frac{V_s}{\omega_s} + \frac{L_m}{L_{ss}} i_{dr} \\ i_{qs} = \frac{L_m}{L_{ss}} i_{qr} \end{cases}, \tag{17}$$

where L_{ss} is the per unit self-inductance of the stator windings.

Therefore, the stator active and reactive powers can also be expressed in terms of the rotor currents as

$$\begin{cases} P_s = V_s \frac{L_m}{L_{ss}} i_{qr} \\ Q_s = V_s \frac{L_m}{L_{ss}} i_{dr} - \frac{V_s^2}{\omega_s L_{ss}} \end{cases} \tag{18}$$

The rotor currents can be derived using the rotor voltages expressed in terms of direct and quadrature components of the rotor currents as in (19).

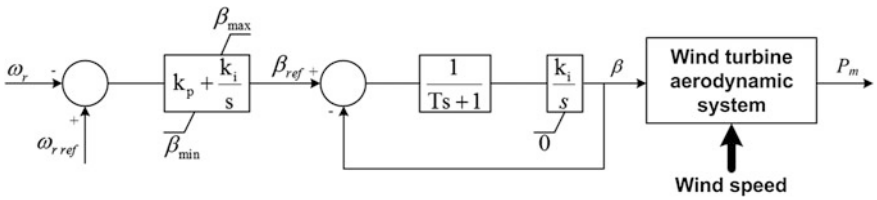

Fig. 2 The pitch control system

$$\begin{cases} \upsilon_{dr} = R_r i_{dr} - s\omega_s\left(L_{rr} - \frac{L_m^2}{L_{ss}}\right) i_{dr} + \left(L_{rr} - \frac{L_m^2}{L_{ss}}\right) \frac{1}{\omega_s} \frac{di_{dr}}{dt} \\ \upsilon_{qr} = R_r i_{qr} + s\omega_s\left(L_{rr} - \frac{L_m^2}{L_{ss}}\right) i_{qr} + \left(L_{rr} - \frac{L_m^2}{L_{ss}}\right) \frac{1}{\omega_s} \frac{di_{qr}}{dt} + \frac{sL_m V_s}{L_{ss}} \end{cases} \tag{19}$$

The Eq. (18) illustrate the decoupling between the WRIG stator active and reactive power control. Thus, the active power can be controlled through i_{qr} while the reactive power can be controlled through i_{dr}. Controlling the frequency converter includes the control systems of both the RSC and GSC, as it can be observed from Fig. 1. Thus, the DFIG control provided by the frequency converter is based on the following control strategy:

- The RSC controls independently the active and the reactive power on the WRIG stator side allowing the machine operation either for a given power factor according to grid requirements imposed by system operators or for voltage control in order to regulate the voltage at the point of common coupling of the WTGS by adjusting the reactive power supply.
- The GSC is controlled to keep the dc-link voltage constant regardless of the magnitude and direction of the active power flow through the rotor circuit. It can also represent a shunt reactive power compensator providing additional voltage control capabilities.

Thus, it was assumed that the RSC behaves like a voltage source inverter whereas the GSC behaves like a current source inverter [7].

2.5 The Pitch Control System

As stated before, the blade pitching control system is primarily used to limit the mechanical power for wind speeds above the rated speed and comprises both the speed controller and the actuator. The speed controller regulates the wind turbine shaft speed to its rated speed, $\omega_{r\,ref}$, and provides the pitch reference angle, β_{ref}, to the actuator, which is responsible to turn the turbine blades to this angle reference, according to the control scheme presented in Fig. 2.

The pitch controller is designed to operate within the limits of the pitch actuator and hence it cannot change the pitch angle too fast or beyond the limits, $\beta_{\min}$ and $\beta_{\max}$ [28]. This means that the blades can only be turned within certain physical

limits, ranging from 0 to 90°, or even a few degrees to the negative side, and the pitch speed is usually less than 5° per second, although it may exceed 10° per second during emergencies [2].

The wind turbine pre-defined optimum power extraction curve can be established for a given k_{opt} associated to an optimum fixed blade angle, β_{opt}, that can be determined for an average short term wind speed forecast. Although, for wind speeds below the rated speed, the optimum pitch angle is in the range of few degrees above zero [2], the minimum limit of the blade angle is usually kept to its optimum value corresponding to $\beta_{\min} = \beta_{opt1}$ in Fig. 2. Also, the speed reference and, thereby, the blade angle reference has to be defined according to the mechanical power extracted from the incoming wind as follows:

$$\begin{cases} \omega_{r\,ref} = \frac{P_{ref}}{T_m} \Rightarrow \beta_{ref} = \beta_{opt1}, & \text{if } P_m \leq P_{\max} \\ \omega_{rref} = \frac{P_{\max}}{T_m} \Rightarrow \beta_{ref} = \beta_{\max}, & \text{if } P_m > P_{\max} \end{cases} \tag{20}$$

where $P_{\max}$ is the mechanical power rating.

2.6 The Rotor Side Converter Control System

The control functions performed by the rotor side converter are derived from Eqs. (18) and (19), aiming the fast dynamic control of both direct and quadrature components of the voltage applied to the rotor circuit in order to assure variable speed operation and independent control of the stator active and reactive power output. Thus, controlling the voltage magnitude allows the electromagnetic torque control, which must follow the speed reference provided by the optimum power-speed extraction curve. In turn, controlling the voltage phase allows the control of the reactive power exchanged with the grid, which in normal operation is set to a given reactive power reference in order to operate the DFIG with a given power factor according to the system operation requirements. In case of grid disturbances leading with voltage sags, if the current in the rotor circuit is not high enough to trigger the crowbar protection system, the RSC will provide voltage control on the point of the DFIG common coupling by adjusting the reactive power supply. Therefore two control approaches have been adopted to represent the RSC dynamics. Under normal operating conditions the RSC is controlled to perform active and reactive power control whereas following grid disturbances the RSC control is set to perform voltage control. These two control approaches are addressed in the following two subsections.

2.6.1 Rotor Speed and Terminal Voltage Control

Due to their simple structure and robustness, Proportional-Integral (PI) controllers have been commonly exploited to generate the $d-q$ components of the rotor

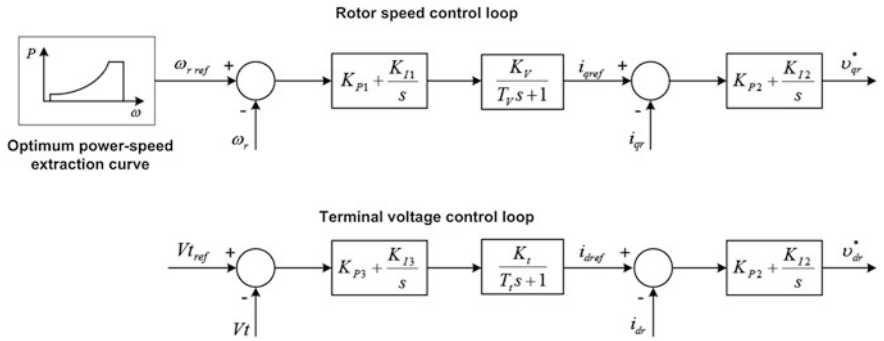

Fig. 3 Control scheme for rotor speed and terminal voltage control loops

voltage references. Thus, taking into account the Eq. (19), two control loops can be defined: The rotor speed control loop and the terminal voltage control loop, according to the control schemes that are presented in Fig. 3.

The speed error determines the quadrature component of the reference current through a PI controller. The required reference of the quadrature component of the rotor voltage can then be obtained through another PI controller. Regarding the terminal voltage control loop, the actual terminal voltage is compared with its reference value and the error is passed through a PI controller to obtain the reference value of the direct current component. This signal is then compared to the *d*-axis actual value and the error is sent to a second PI controller, which outputs the reference for the direct component of the rotor voltage.

Besides the above mentioned PI controllers, additional control blocks were included in order to represent the nonlinear and coupling terms that characterize the dynamic behaviour of the generator rotor according to Eq. (19). As discussed in [7], these control blocks improve the performance of the controllers during severe grid disturbances. The involved parameters, K_v, K_t, T_v and T_t should be derived from the machine parameters.

2.6.2 Active and Reactive Power Control

As already mentioned previously, during normal operation the RSC is set to control the active and reactive power independently. Thus, two control loops have been commonly adopted to derive the reference components of the rotor voltage [12]: The active power control loop and the reactive power control loop, as it can be observed from Fig. 4. These control loops are also defined based on Eqs. (18) and (19) exploiting PI controllers to derive the *d*–*q* components of the rotor voltage. However, in this control design, the additional control blocks representing the coupling and the nonlinear terms were not considered, since the involved time constants derived from the machine parameters are typically very small and therefore, under these circumstances, their effect on the RSC performance can be neglected.

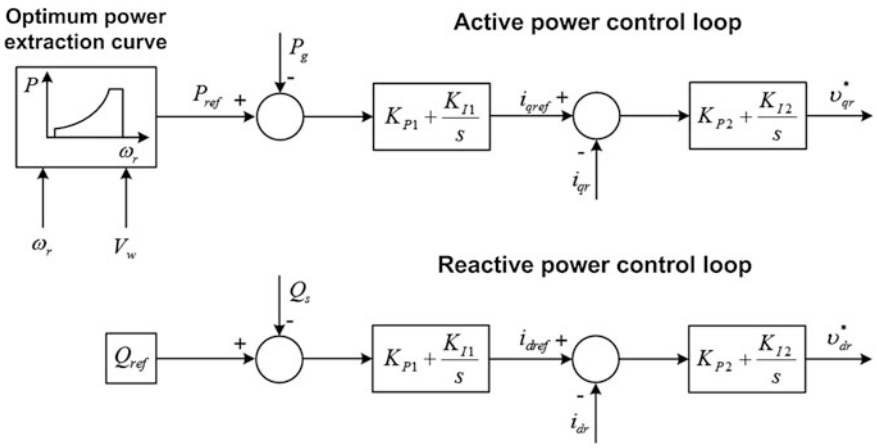

Fig. 4 Control scheme for active and reactive power control loops

The reference active power is provided by the maximum power extraction curve, given by Eq. (13), according to the actual generator speed in order to assure the DFIG operation at the maximum aerodynamic efficiency while the reactive power reference is set to a given set-point which can be controlled according to grid requirements imposed by system operators. The rotor voltage components are then obtained from two separate sets of PI controllers involving a cascade structure, in which the outer PI controllers are used to regulate the references of the rotor current components i_{dref} and i_{qref}, and the inner side PI controllers are used to regulate the υ^*_{qr} and υ^*_{dr} components, respectively.

The rotor reference voltage components provided by the RSC control scheme are transformed to *abc* coordinates through the Park's inverse transformation [26] and sent to the PWM signal generator of the converter in order to control the IGBT switching, as represented in Fig. 5.

It should be stressed that in power stability studies the power electronic interfaces are commonly represented by a fundamental frequency approach based on their control functions only, so that switching transients, harmonics and inverter losses are neglected since fast transient phenomena are not relevant for the purpose under analysis. However, converter losses and filters can be added by specifying the series impedance to the frequency converter [13, 17, 31, 41].

2.7 The Grid Side Converter Control System

Under normal operating conditions, the GSC is controlled to keep the dc-link voltage constant and to assure the converter operation with a unity power factor. When the DFIG is set to provide voltage control following grid disturbances, the

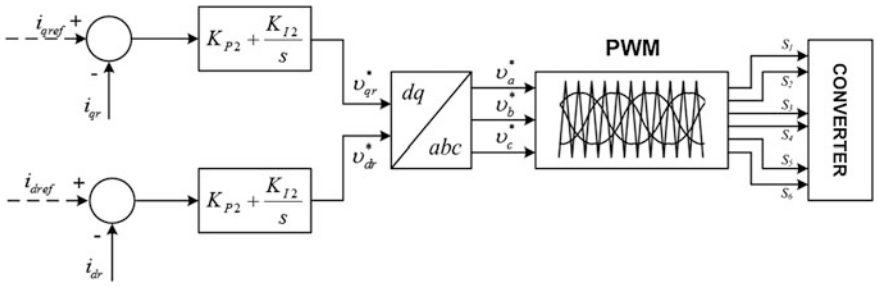

Fig. 5 Control scheme of the IGBT switching

reactive power demand is assigned to the GSC when the RSC is blocked, due to the co-ordinated voltage control, as already mentioned previously. Therefore, the reactive power reference for the GSC is set to its limit, so that the converter will contribute with its maximum reactive power to perform voltage support. Thus, the GSC control strategy comprises a fast inner current control loop to control the current injected to the grid following a predefined reactive power reference, and an outer slower control loop that controls the dc-link voltage, allowing that the energy delivered to the dc-link capacitor is transferred either to the utility system or to the RSC depending upon the DFIG operation in sub synchronous or super synchronous mode, respectively.

The current control loop is implemented using the instantaneous power theory proposed in [3] for active power filters control. Thus, according to Fig. 6, the instantaneous voltages and currents in three-phase circuits, v_{abc} and i_{abc}, respectively, expressed as instantaneous space vectors, are easily transformed to α–β–0 coordinates as follows:

$$\begin{bmatrix} v_0(t) \\ v_\alpha(t) \\ v_\beta(t) \end{bmatrix} = C \times \begin{bmatrix} v_a(t) \\ v_b(t) \\ v_c(t) \end{bmatrix} \quad \text{and} \quad \begin{bmatrix} i_0(t) \\ i_\alpha(t) \\ i_\beta(t) \end{bmatrix} = C \times \begin{bmatrix} i_a(t) \\ i_b(t) \\ i_c(t) \end{bmatrix} \tag{21}$$

where C is the Clark transformation given by

$$C = \sqrt{\frac{2}{3}} \times \begin{bmatrix} 1/\sqrt{2} & 1/\sqrt{2} & 1/\sqrt{2} \\ 1 & -1/2 & -1/2 \\ 0 & \sqrt{3}/2 & -\sqrt{3}/2 \end{bmatrix} \tag{22}$$

So, as described in [9], the instantaneous active and reactive powers are defined as:

$$\begin{bmatrix} p(t) \\ q(t) \end{bmatrix} = \begin{bmatrix} v_\alpha(t) & v_\beta(t) \\ -v_\beta(t) & v_\alpha(t) \end{bmatrix} \times \begin{bmatrix} i_\alpha(t) \\ i_\beta(t) \end{bmatrix} \tag{23}$$

where $p(t)$ is the instantaneous active power (W) and $q(t)$ is the instantaneous reactive power (VAr).

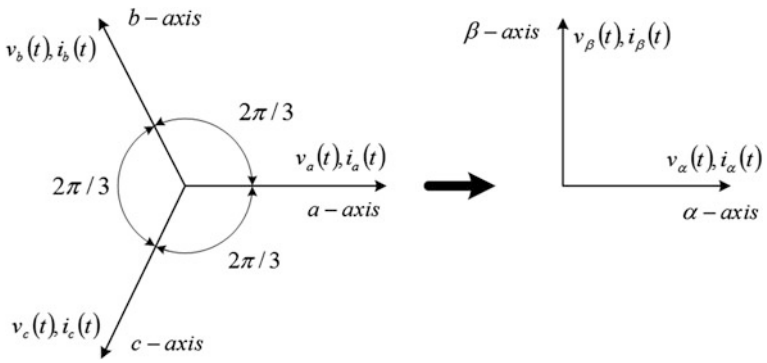

Fig. 6 *abc* to α–β coordinates transformation

The current reference signals i_a^*, i_b^* and i_c^* employed to turn on and to turn off the switches of the PWM based current source inverter are obtained instantaneously from Eq. (23) as follows:

$$\begin{bmatrix} i_{ca}^* \\ i_{cb}^* \\ i_{cc}^* \end{bmatrix} = \sqrt{\frac{2}{3}} \times \begin{bmatrix} 1 & 0 \\ -1/2 & \sqrt{3}/2 \\ -1/2 & -\sqrt{3}/2 \end{bmatrix} \times \begin{bmatrix} v_\alpha(t) & v_\beta(t) \\ -v_\beta(t) & v_\alpha(t) \end{bmatrix}^{-1} \times \begin{bmatrix} p_c(t) \\ q_c(t) \end{bmatrix} \tag{24}$$

where $p_c(t)$ and $q_c(t)$ are, respectively, the instantaneous active and reactive power on the GSC terminals, $v_\alpha(t)$ and $v_\beta(t)$ are the stator voltage in α–β coordinates, respectively.

In balanced three-phase systems the instantaneous active and reactive powers are constant and equal to the three-phase active and reactive powers, respectively [9]. Thus, $q_c(t)$ in Eq. (23) corresponds to the reactive power reference that assures the required power factor and $p_c(t)$ is the active power flow through the rotor circuit. Neglecting losses and the switching harmonic frequencies on the inverter output currents, the energy stored in the dc link capacitor can be obtained as [9]:

$$E_c = \int_{-\infty}^{t} (p_r(t) - p_c(t))dt = \frac{1}{2} C_{dc} v_{dc}^2(t) \tag{25}$$

where $p_r(t)$ is the RSC instantaneous power output, C_{dc} is the dc-link capacity (F) and $v_{dc}(t)$ is the dc capacitor instantaneous voltage (V).

The above equation shows that the dc-link voltage deviations depend on the power balance. If this voltage is kept constant $p_c(t) = p_r(t)$ and the active power exchanged with the grid corresponds to the RSC active power output. Thus, according to [5], the full control strategy of the rotor side converter is represented through the control scheme depicted in Fig. 7.

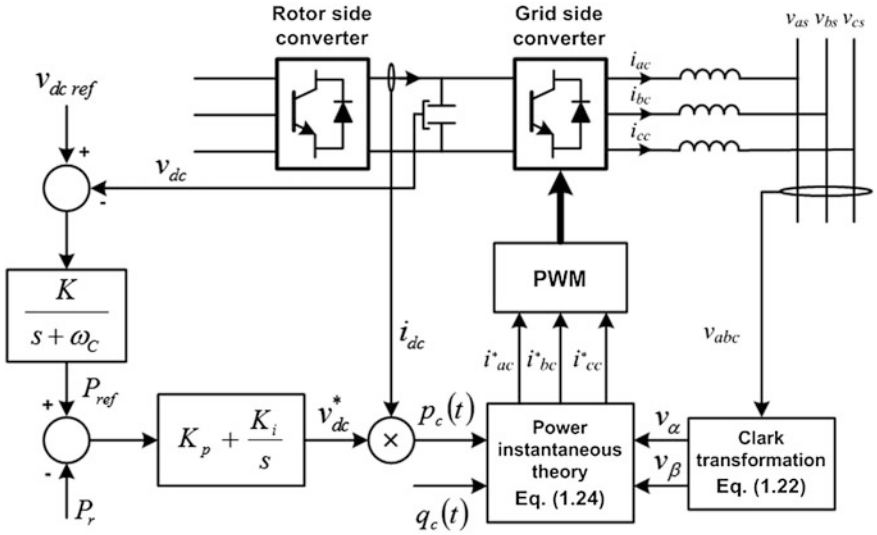

Fig. 7 The rotor side converter control scheme

As it can be observed from Fig. 7, the reference signal of the RSC output power is derived from the error between the reference value of the dc-link voltage and its current value through a controller defined as a proportional gain together with a low pass filter to eliminate the switching harmonics in the dc-link voltage.

3 Using Fuzzy Control to Improve DFIG Fault Ride Through Capability

To keep the RSC in operation plays an important role to improve FRT capability of DFIG and, therefore, the network dynamic behaviour following disturbances successfully eliminated, as reported in [39, 47, 53]. Therefore, the limitation of the generator currents under these circumstances has been a matter of concern regarding the RSC control design, since a robust control of the WRIG can prevent the crowbar trigger [7, 13]. However, the DFIG performance depends upon the suitable choice of the PI gains used in the RSC control system that is based on physical insights. Thus, tuning PI gains for performance optimization is a very hard task since the nonlinearities involved in the DFIG dynamics require a carefully tuning procedure for different operating conditions. Furthermore, the complexity level of this task will increase when the DFIG is connected to large power systems, due to the system dimension, or to an isolated system due to the stronger coupling between active and reactive powers [7].

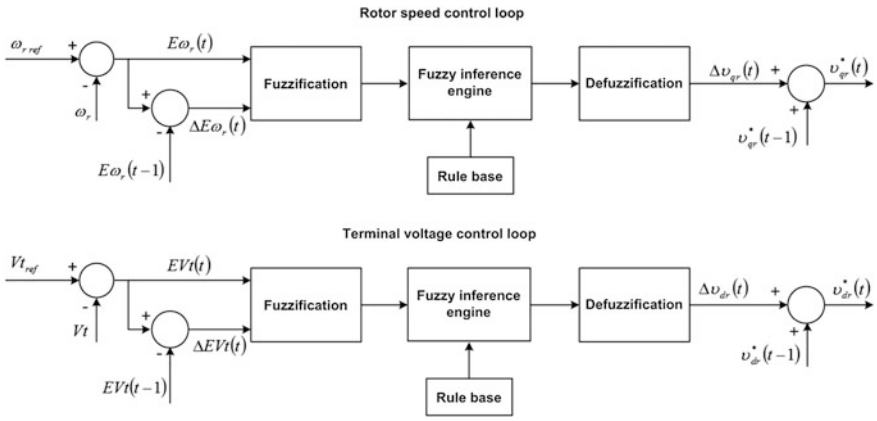

Fig. 8 Block diagram of the fuzzy controller

Fuzzy control provides a systematic way to control nonlinear processes based on the human experience, being considered as a heuristic approach that can improve the performance of closed loop systems. When properly designed, fuzzy controllers can perform better than conventional PI controllers when used for control purposes of nonlinear dynamic systems [27, 40].

Due to their robustness, the design of two fuzzy controllers is proposed in this section as an alternative control strategy of the RSC based on PI controllers. The performance of this approach is then evaluated by comparison with the performance of the conventional PI based approach. For this purpose, the whole DFIG dynamic model presented in Sect. 2 together with the designed fuzzy control approach were embedded in the full dynamic simulation tool and dynamic simulations were carried out considering the occurrence of disturbances.

3.1 Fuzzy Controllers Design

As the RSC control system is set to perform voltage control, the fuzzy control strategy comprises two controllers: The rotor speed controller and the terminal voltage controller. Their structures are similar, comprising the fuzzy inference engine and the defuzzification block [52] as depicted in Fig. 8. All the inputs and outputs are expressed in per unit referred to the system bases.

The number and the form of the membership functions defining the fuzzy inputs and outputs of both controllers were defined off-line and the universe of discourse for each variable was normalized to distinct values according with the behaviour of the corresponding variables observed during dynamic simulations. Standard triangular membership functions were adopted for both the input and output of the fuzzy sets of both fuzzy controllers. The designed fuzzy sets for rotor speed control and terminal voltage control are presented in Fig. 9.

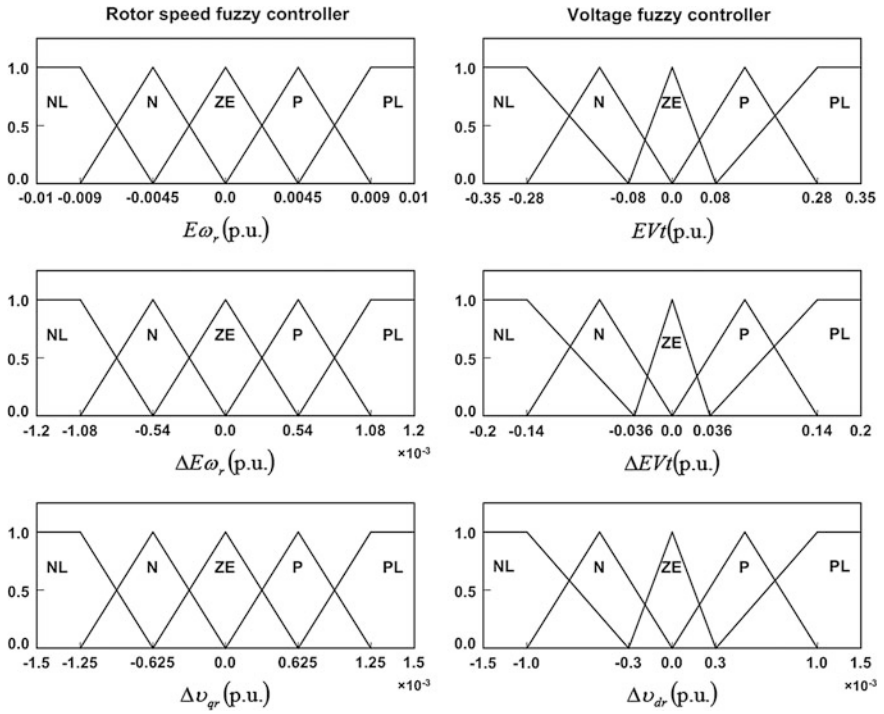

Fig. 9 Triangular membership functions for inputs and outputs fuzzy sets of fuzzy controllers

Table 1 Rule base for rotor speed fuzzy controller and reactive power fuzzy controller

		$\Delta E\omega_r$							ΔEVt				
		NL	N	ZE	P	PL			NL	N	ZE	P	PL
$E\omega_r$	NL	PL	PL	PL	P	ZE	EVt	NL	NL	NL	NL	N	ZE
	N	PL	PL	P	ZE	N		N	NL	NL	N	ZE	P
	ZE	P	P	ZE	N	N		ZE	N	N	ZE	P	P
	P	P	ZE	N	NL	NL		P	N	ZE	P	PL	PL
	PL	ZE	N	NL	NL	NL		PL	ZE	P	PL	PL	PL

As it can be observed from Fig. 9, the fuzzy sets were defined as: *NL*—Negative Large, *N*—Negative, *P*—Positive, *PL*—Positive Large and *ZE*—Zero. The control rules of the fuzzy controllers are commonly represented through a set of heuristically chosen rules. In this case, the designed fuzzy rules for both controllers are presented in Table 1.

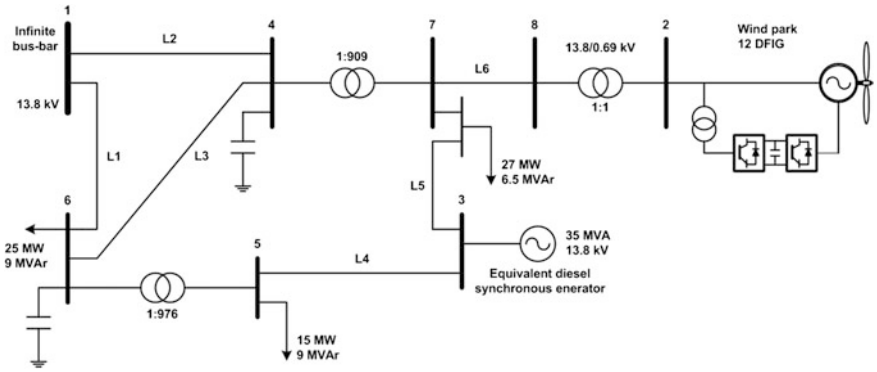

Fig. 10 Test system single line diagram

3.2 The Test System

In order to evaluate the impact of the RSC control strategy based on fuzzy controllers on the power system dynamic behaviour, comparative tests with the PI controllers have been performed through dynamic simulations considering the occurrence of a grid disturbance in the test system depicted in Fig. 10.

For simulation purposes, a dedicated dynamic power system simulation software package was developed under *MATLAB*^{TM} environment. The full power system dynamic model involves the mathematical representation of the utility grid, the wind park equipped with 12 DFIG operating under similar conditions and the equivalent diesel synchronous generator connected to bus 3.

The general multimachine power system model developed in [52] is used to define, in a compact form, the transmission network and the stator equations of the machines. The synchronous generator of the equivalent diesel group is represented through a fourth order transient model [26] together with both the automatic voltage regulator (IEEE type 1) and the speed governor. Additionally, a simple first order model is used to represent the diesel engine dynamics, as reported in [52]. The wind park is represented through a dynamic equivalent model corresponding to the twelve DFIG, whose dynamics are represented through the mathematical model described in Sect. 2.

It must be stressed that RSC control aims to perform rotor speed and terminal voltage reference tracking and thereby it is based on both the speed and terminal voltage control loops presented in Sect. 2.6.1. Then, the PI gains were carefully adjusted using trial and error approaches in order to obtain minimum variations of the design variables, considering the simulation of the above mentioned disturbances taking place on test system depicted in Fig. 10. After the long process of tuning, the derived PI gains are presented in Table 2 together with the other parameters, which were obtained based on the machine characteristics.

Table 2 Parameters of the RSC controller using PI controllers

K_{P1}	K_{I1}	K_{P2}	K_{I2}	K_{P3}	K_{I3}	K_v	K_t	T_v	T_t
20.27	15.76	0.0443	0.0032	15.06	10.50	0.0321	0.0321	0.4434	0.4434

The DFIG operating conditions correspond to a constant wind speed of 15 m/s, such that the rotor speed equals 1.01 p.u. The terminal bus voltage is set to 1.02 p.u. Regarding the GSC, the reactive power set point is set to its maximum value in order to provide additional reactive power injection through the rotor circuit. The results obtained are presented in the following section.

3.3 Simulation Results and Discussion

In order to evaluate the performance of both PI and fuzzy controllers with respect to the rotor current behaviour, which could trigger the crowbar protection, a three-phase short circuit taking place on bus 6 of the test system was simulated at $t = 1$ s with a typical clearing time of 100 ms. It was assumed that the crowbar will be triggered if the rotor current increases above 1.25 kA (0.18 p.u. on the WRIG base) and that the DFIG will be disconnected from the grid when the terminal voltage is outside the range $0.7 < Vt < 1.15$ p.u. The definition of voltage and current limits was based on the rating of both the generator and the frequency converter. The results obtained following the short circuit occurrence are presented in Fig. 11.

As it can be observed from Fig. 11a, the fuzzy controllers would be able to keep the machine connected to the grid while the PI controllers will lead to the voltage protection actuation since the upper voltage limit was exceeded, as it can be observed from Fig. 12c. On the other hand, the rotor current will trigger the crowbar protection and therefore the DFIG operating conditions will be changed. If the protection regulation settings were stricter and the controllers were not able to damp the current oscillations, the crowbar could be triggered several times due to the current overshoot following the RSC re-connection attempt and, therefore, the DFIG performance will become worsened. The DFIG electromagnetic torque can be observed from Fig. 11b. Large oscillations can be experienced by the machine when controlled by PI controllers as a result of the crowbar operation. During the short circuit the fuzzy controllers perform better, in spite of the fact that the membership functions were not carefully adjusted as in the PI controller design.

For large control inputs, leading to large variations with respect to the reference values, fuzzy controllers usually perform better than PI controllers while similar performances have been achieved for small input variations [30]. Therefore, although no optimization methods were used for both kinds of controllers, fuzzy controllers present a better whole performance regarding systems subjected to severe disturbances as in power systems applications.

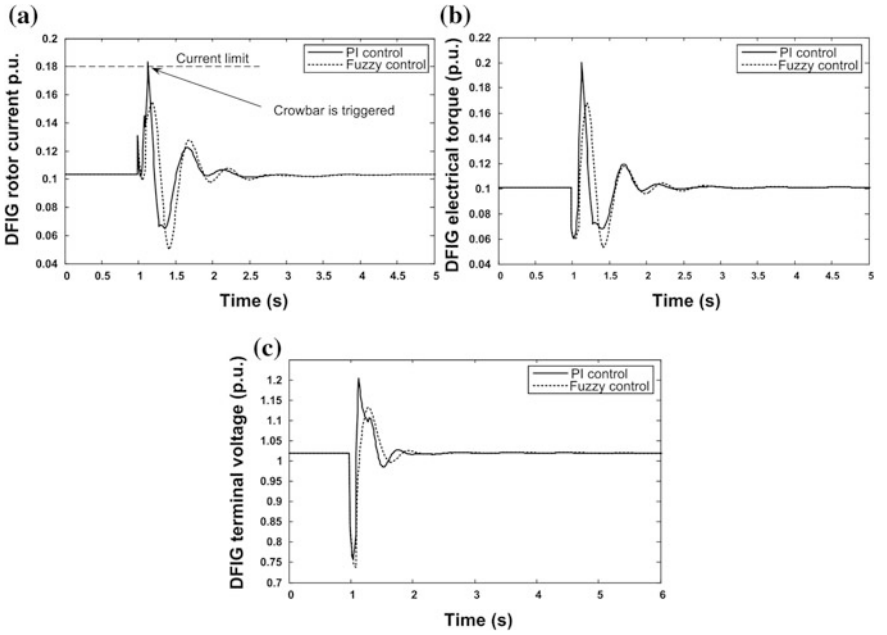

Fig. 11 DFIG behaviour following a three-phase short-circuit: (**a**) rotor current; (**b**) electrical torque; (**c**) terminal bus voltage

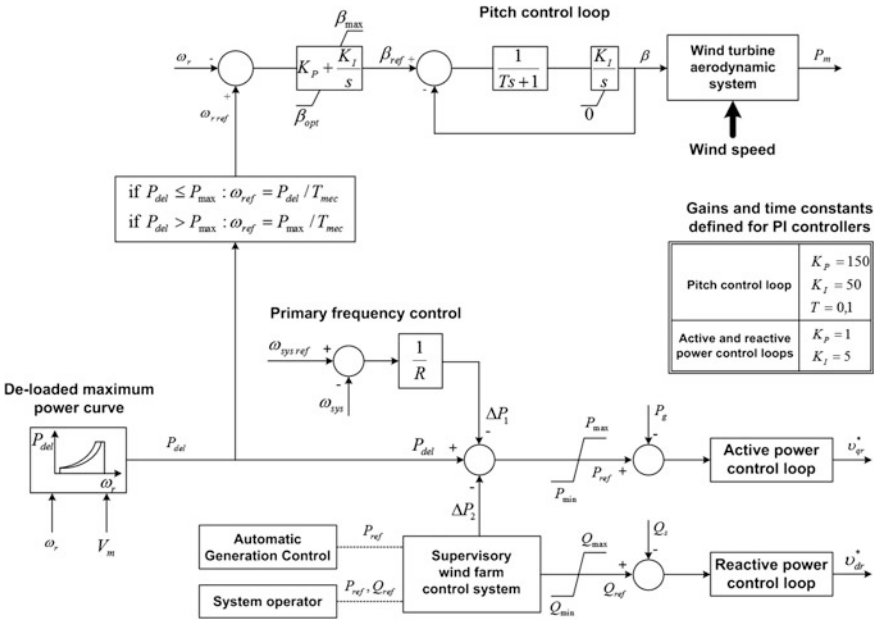

Fig. 12 Full frequency control strategy of the DFIG rotor side converter

Although PI controllers could play an important role regarding the DFIG behaviour following ac grid disturbances, they must be carefully designed. This is a very difficult task due to the presence of nonlinear and coupling terms on the mathematical equations representing the dynamics of DFIG. Also, a large amount of dynamic simulations is required to meet the acceptable range of PI gains. In contrast, fuzzy controllers were adjusted in just a few simulations.

4 Participation of DFIG in System Frequency Regulation

Regarding the potential of wind parks to participate effectively in primary frequency regulation, several research works have been developed aiming DFIG to contribute for inertia control and for primary frequency control [14, 20, 22, 25, 37].

Inertia control can be provided through a supplementary inertial control loop [14] exploiting the kinetic energy stored in the rotating mass of wind turbines, such that the additional amount of power supplied by the DFIG to the grid is proportional to the derivative of the system frequency. Nevertheless, the inertia control is similar to the one commonly used in synchronous generators [9, 25], being the droop loop used to change the active power injected by the DFIG proportionally to the frequency deviation. In [37] both frequency control schemes are exploited, but the droop loop is only activated when the system frequency exceeds certain limits. Moreover, in order to provide inertia control, the DFIG has to be de-loaded, meaning that there is a margin to increase the active power output during large low frequency periods. Thus, in [22], the pitch angle controller was exploited to develop a primary frequency control strategy that allows the DFIG to provide a proportional frequency response. For this purpose the active power injected by DFIG is adjusted through the regulation of the minimum pitch angle according to the frequency deviation.

In this section, a robust primary frequency control approach for DFIG is presented. Following a system frequency deviation an active power injection takes place through the initial leading action of the RSC. The pitch control system is further used in order to adjust the mechanical power accordingly. The amount of the injected active power is defined from the proportional frequency regulation loop together with a power reference adjustment obtained from a de-loaded power curve such that a new equilibrium point of operation can be obtained following frequency changes. The effectiveness of this control approach was tested in a small isolated power system when the wind generation plays an important role.

4.1 The DFIG Frequency Control Approach

In order to allow DFIG participation in frequency regulation the adopted control approach focuses on the RSC control strategy, which is designed to perform

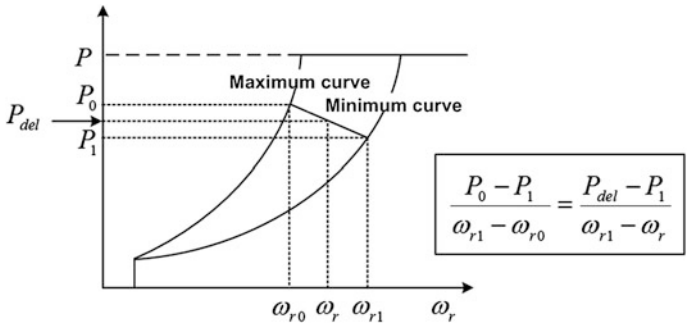

Fig. 13 Schematic diagram of de-loaded optimal active power curve

directly active and reactive power control, as presented in Sect. 2.6.2. The GSC operates at a unitary power factor and controls the dc-link voltage, according to the control scheme presented in Sect. 2.7.

Besides the active and reactive power control loops, the full control approach of the RSC comprises also the primary frequency control loop that defines the ΔP_1 set point, as a result of system frequency changes, a pitch control strategy and a control block associated to an external supervisory wind farm control system, as it can be observed from Fig. 12.

DFIG are required to respond to a request from the system operator, due to an Automatic Generation Control (AGC) demand or because the operational reasons related with the need to control power flows in the network area, through the supervisory wind farm control block. This request leads to an optimized adjustment of the active power output of the individual DFIG inside the wind park [4] defining thus the ΔP_2 set-point.

The active power control loop allows the DFIG tracking the power reference, P_{del}, obtained from the de-loaded maximum power curve [6], defined in terms of the DFIG reserve capacity to be available for inertia control. This reference power is also used to adjust the rotor speed through the pitch control loop, as illustrated in Fig. 13.

The adoption of a power reference derived from the de-loaded power extraction curve allows the increase of the DFIG active power generation when the system frequency decreases as a result of either a sudden load increase or a large generation facility loss. Thus, from Fig. 13, the power reference can be defined as:

$$P_{del} = P_1 + \frac{P_0 - P_1}{\omega_{r1} - \omega_{r0}}(\omega_{r1} - \omega_r), \tag{26}$$

where P_0 and P_1 are the maximum and the de-loaded active powers for a given wind speed, respectively, being ω_{r0} and ω_{r1} the minimum and the maximum rotor speeds referred to the generator side, respectively.

The relationship between P_0 and P_1 is defined as

$$P_1 = k_{del} P_0, \tag{27}$$

where $k_{del} = 1 - \frac{\%\ \text{de–loading}}{100}$, $P_1 = k_{opt1}\omega_{r1}^3$, $P_0 = k_{opt0}\omega_{r0}^3$ with k_{opt1} and k_{opt0} being the optimum constants given by Eq. (14) for both maximum and minimum power curves, respectively.

From the above equations, the reference power can be written as

$$P_{del} = \frac{(\omega_r - \omega_{r0})k_{del} + \left[\left(\frac{k_{del}k_{opt0}}{k_{opt1}}\right)^{1/3}\omega_{r0} - \omega_r\right]}{\left[\left(\frac{k_{del}k_{opt0}}{k_{opt1}}\right)^{1/3} - 1\right]\omega_{r0}} P_0 \tag{28}$$

Assuming that P_0 and ω_0 are previously known, the reference power depends basically of the rotor speed ω_r referred to the generator side according to Eq. (20).

Like in a conventional synchronous generator, the primary frequency control integrated into the rotor side active power control loop comprises a droop loop, characterized by a regulation R expressed in per unit in the system base, which is responsible to change the DFIG injected active power, P_g, following a system frequency deviation [6] as

$$P_g = P_{del} - \frac{1}{R}\left(\omega_{sys} - \omega_{sys\_ref}\right), \tag{29}$$

where ω_{sys} and ω_{sys_ref} are the system frequency and its rated value, respectively.

The injected power increment requires a new operating point defined through a new rotational speed and the corresponding mechanical power according to the turbine power curve for the incoming wind speed. So this control strategy is complemented with the pitch control system (used together with the frequency converter control) by adjusting the rotor speed referred to the generator side, ω_{r_ref}, according to the de-loaded maximum power curve taking into account the operational conditions, as presented in Fig. 12.

4.2 The Test System

The effectiveness of the proposed primary frequency approach was evaluated using a test system comprising 5 DFIG (660 kW each) installed in a wind park connected to an isolated grid represented by a single bus with a synchronous thermal unit rated at 10 MW, as it can be observed from Fig. 14.

The WRIG mathematical model described in Sect. 2.3 together with both the RSC full frequency control strategy depicted in Fig. 12 and the GSC control presented is Sect. 2.7, was embedded in the dedicated dynamic simulation package already used in Sect. 3.2. The thermal unit was also represented by the dynamic model adopted in Sect. 3.2, considering that the frequency droop of the generator is 4 % in the machine base and that the integral control loop allows the system to

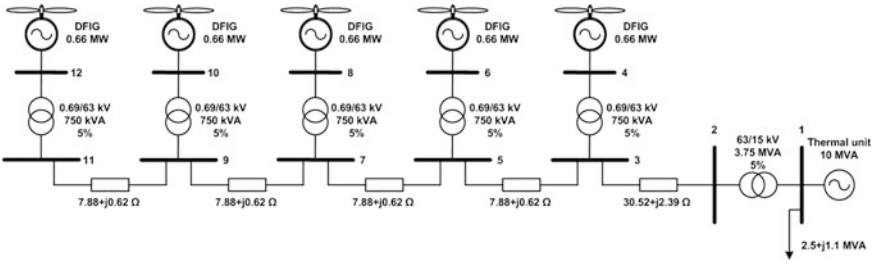

Fig. 14 Single line diagram of the test system

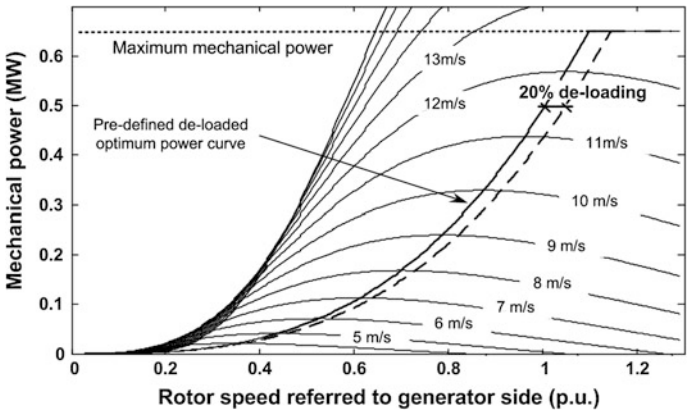

Fig. 15 De-loaded optimal power curve adopted for each DFIG

recover frequency to its nominal value following unbalances between load and generation, being the integral control gain of 4.5 p.u. in the system base power.

4.3 Simulation Results and Discussion

A de-loaded margin of 20 % was adopted for each DFIG, providing in this way a 20 % generation reserve available for the entire wind speed range, as it can be observed from Fig. 15.

For simulation purposes, it was assumed that the wind speed was 12 m/s in the entire wind park. Because of an operator request, all wind generators are operating in the minimum optimum curve (dotted line in Fig. 15), corresponding to 458 kW. In addition, the droop, R, of the DFIG primary frequency control loop was considered as 5 % with respect of the machine base. It was also assumed that the GSC reactive power reference is set to zero in order to assure the GSC operation with a unitary power factor.

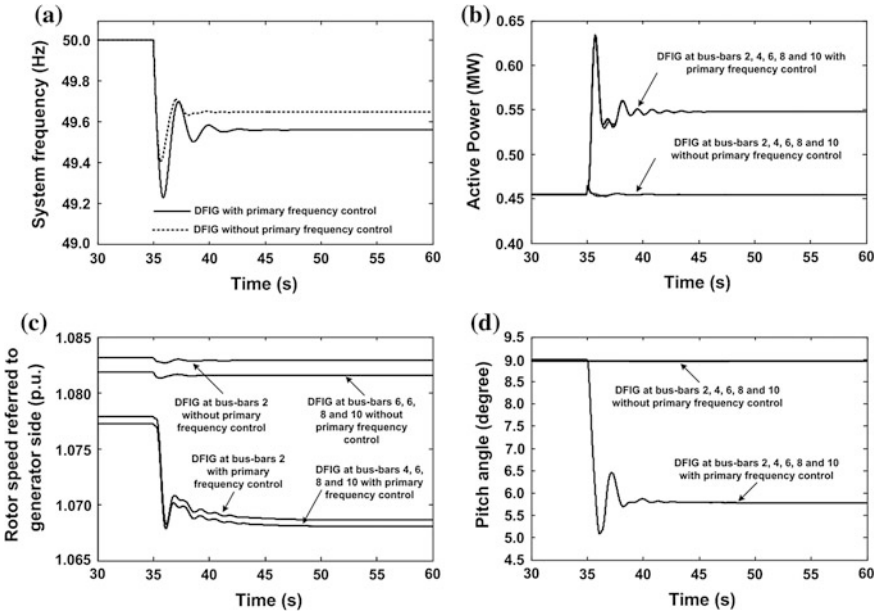

Fig. 16 DFIG dynamic behaviour considering the thermal unit without frequency control: (**a**) frequency behaviour; (**b**) active power; (**c**) rotor speed; (**d**) pitch angle

A change in load value was simulated at $t = 35$ s by increasing the load connected at bus 1 in 80 % leading with a system frequency deviation. In order to show the DFIG capability of keeping up part of the load increase it was assumed that the integral frequency control loop of the thermal unit was not in operation, being this situation similar to the initial periods following a system disturbance when only primary frequency control operates while expecting for AGC to correct the frequency drift.

The system frequency dynamic behaviour is presented in Fig. 16a, considering that the DFIG provides frequency control (dotted line) and considering that it is not participating in this control (full line). It can be clearly observed that the frequency excursion is smaller when the wind generators are participating in grid frequency control. The DFIG dynamic behaviour regarding active powers, rotor speeds and pitch angles with and without primary frequency control is presented in Fig. 16a, b and c, respectively.

When DFIG do not participate in frequency control, only minor changes in active power outputs and rotor speed behaviours can be observed, as a result of induced changes in the electrical torques of these units resulting from changes in network voltages following load changes. When frequency control is activated, the DFIG increases fast the active power output in order to compensate the system load increase. Therefore, the DFIG rotor speed decreases following the de-loaded extraction power curve. As a result, the pitch angle is decreased, allowing the

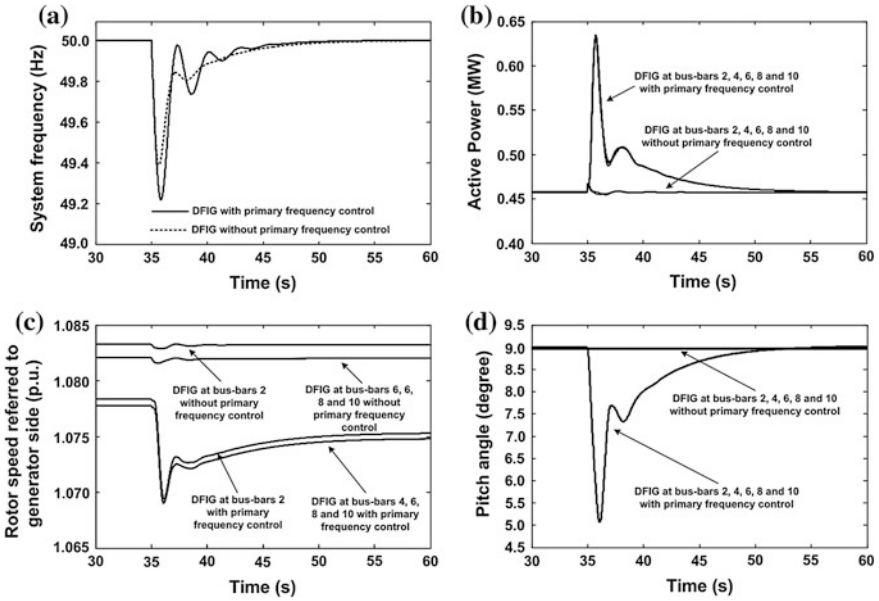

Fig. 17 System frequency behaviour considering the thermal unit with frequency control

increase of the mechanical power extracted from the incoming wind speed. Therefore, after the initial transients, these variables stabilize in a different value than the initial one. The results allow concluding that the system behaviour is considerably improved in terms of the frequency deviations when DFIG participates in frequency control.

In order to highlight the DFIG dynamic behaviour, similar results considering the presence of the integral control loop in the speed governor of the thermal unit are presented in Fig. 17. Grid frequency behaviour is presented in Fig. 17a, showing that the integral control action of the thermal unit governor brings the system frequency to its nominal value. Figure 17b, c and d show the behaviour of active powers, rotor speeds and pitch angles of the DFIG.

From these results one can conclude that when DFIG participates in primary frequency control the frequency deviations are smaller and better damped due to the fast operation of the RSC. Thus, the presence of DFIG operating with primary frequency control can contribute to increase the system robustness with particular benefits for isolated power systems. On the other hand, DFIG can provide frequency control as an ancillary service to help supporting frequency when large disturbances occur. Such a service can be required during operation scenarios where conventional power plants have a smaller presence, like during valley hours with a large amount of wind generation.

5 Robust Tuning of PSS to Installed in DFIG

Power system stabilisers installed in DFIG can be used to provide additional damping to the electromechanical modes of oscillation, which are related to low frequency (0.1–2 Hz) power oscillations occurring among the rotors of the synchronous machines as a result of either some controller settings or large power flows through weak transmission lines. However, DFIG will contribute effectively for this purpose only if the oscillation mode is controllable through power injection on the DFIG terminals and observable through the PSS input signals. Moreover, the performance of PSS installed in DFIG is significantly affected by the system operating conditions resulting from different wind speeds [33]. Therefore, it is desirable to find a trade-off solution that will provide a set of parameters for each PSS able to assure an acceptable damping level for all operating scenarios. This solution is commonly known as a robust solution.

Due to the large number of operating scenarios and taking into account that PSS installed in DFIG add damping indirectly, a robust solution may be quite difficult to achieve. Additionally, some care should be taken in order to assure that the PSS does not change the modes of oscillation of the DFIG affecting its performance. Thus, in this section, a heuristic approach is presented in order to perform a simultaneous robust tuning of the several PSS installed in DFIG involving a very large set of scenarios that represent different operating conditions. For this purpose an optimization problem will be solved pursuing the minimization of PSS action so that the minimum acceptable damping is achieved for a representative set of scenarios. The mathematical model of DFIG equipped with PSS as well as the algorithm to perform PSS robust tuning is presented in this section. The effectiveness of the robust solution is evaluated using a suitable test system. The results obtained are also presented and discussed.

5.1 Model of DFIG with PSS

The mathematical model of DFIG with PSS is based on the DFIG model presented in Sect. 2, representing the fundamental dynamics of a WRIG, a wind turbine with pitch angle control and a RSC control system based on both active and reactive power control loops, as depicted in Fig. 18. The dynamics of the GSC were not considered.

As it can be observed from Fig. 18, the PSS output is a stabilizing signal to be summed to the quadrature component of the rotor voltage in the active power control loop. This signal is responsible to create a generator damping torque in phase with the rotor speed through the active power modulation [3], where the DFIG acts as an amplifier of the controller similarly to synchronous machines when used for the same purpose [48].

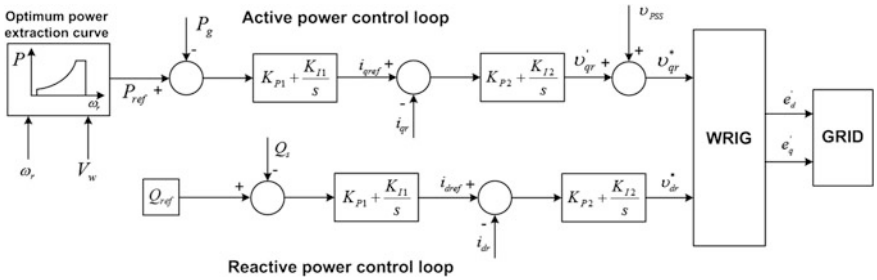

Fig. 18 Control scheme of DFIG with PSS

Assuming that the pitch angle is constant during the studied period, the DFIG state space model suitable for modal analysis is derived from its detailed model through the linearization of the differential equations describing both the WRIG fundamental dynamics and the ones related with the RSC based PI controllers, being given by [33]:

$$\Delta \dot{x} = A_1 \Delta x + B_1 \Delta \upsilon_s + C_1 \Delta P + D_1 \Delta \upsilon_r, \tag{30}$$

This equation is then defined as a function of state variables x, terminal voltage υ_s, active power P and rotor voltage υ_r. The terms related with active power and rotor voltage must be eliminated after deriving the following algebraic equations:

$$\begin{cases} \Delta P = A_2 \Delta x + B_2 \Delta \upsilon_s + D_2 \Delta \upsilon_r \\ \Delta \upsilon_r = A_3 \Delta x + B_3 \Delta \upsilon_s + C_3 \Delta P \end{cases} \tag{31}$$

After some mathematical transformations the DFIG state space model can be written in the canonical form as:

$$\begin{aligned} \Delta \dot{x} &= A \Delta x + B \Delta \upsilon_s \\ \Delta i &= C \Delta x + D \Delta \upsilon_s \end{aligned} \tag{32}$$

This kind of models regarding synchronous machines and DFIG are combined with the network equations in a multi-machine system model and the state matrix is then used to perform standard modal analysis [33]. The damping conditions associated to each mode of oscillation are determined from the state matrix eigenvalues exploiting QR method routines from MATLAB™.

The configuration of PSS to install in DFIG is presented in Fig. 19.Here K is the PSS gain, T_w is the time constant of the washout filter used to prevent the PSS from responding to steady-state changes of the input signal and the time constants T_1–T_4 are used in the lead-lag blocks in order to provide the necessary phase compensation. Since the PSS output is added to the quadrature component of the rotor voltage, a limitation block is also included in the PSS scheme, being the maximum and minimum limits established according to the machine operation.

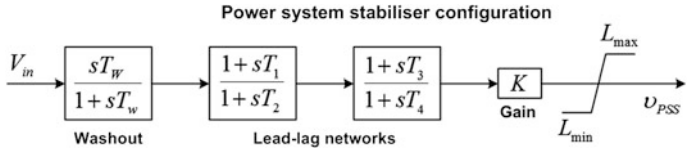

Fig. 19 Power system stabiliser configuration to be installed in DFIG

Regarding the PSS inputs, residue analysis should be used in order to select the most adequate signals among rotor speed, voltage, electrical power and electrical frequency. However, from the physical insights acquired when dealing with this problem, the input signals that perform best are voltage and frequency. In fact, due to the decoupling between grid and DFIG provided by the RSC controller, rotational speed and electrical power are less sensitive to oscillations that occur in the grid and usually do not contain sufficient information about the mode of oscillation to damp by the PSS.

5.2 Methodology for PSS Robust Tuning

The importance of PSS tuning and how this task may be affected by the increase of wind power integration has been stressed and several methods have been used for this purpose. However, they are not suitable to find a robust solution for a very large number of scenarios. Meta-heuristics based optimization algorithms can find robust solutions but require too much computational effort [32]. In contrast, sensitivities based methods require less computational effort but do not assure that a robust solution will be found [42]. Therefore, the methodology adopted for PSS robust tuning is based on a meta-heuristic approach.

The PSS parameters are determined by solving an optimization problem with capability to deal with several operational requirements which are modelled in the objective function or considered as constrains. The mathematical formulation is derived from the method presented in [32] that pursues the minimization of the PSS gain in order to provide the minimum acceptable damping. As a result a low stabilizer gain is obtained reducing thus the effect of the limitation block in the stabilizer output [42] in contrast with the alternative formulations, which aim the damping maximization [46]. For a given scenario k, the problem can then be formulated through the following objective function aiming the minimization of a quality index, Q_k as [33]:

$$\min Q_k(X) = \sum_{i=1}^{nm} \sum_{j=1}^{ng} \left(w_{ji} K_j + W N_j \alpha_j \right), \tag{33}$$

subjected to

$$\varsigma_i \geq \varsigma_{i\min} \tag{34}$$

$$|\Delta f_i| \leq \Delta f_{i\min} \tag{35}$$

$$X_{j\max} \geq X_j \geq X_{j\min}, \tag{36}$$

where X represents the solution of the problem corresponding to the values of the parameters for the several PSS to be installed, nm is the number of modes, ng is the total number of generators, w is a weighting factor, K is the PSS gain, W is a penalty factor to weight phase compensation, N is the number of lead-lag blocks, α is the filtering ratio, ς is the damping and Δf is the eigenvalue frequency change. The subscript i is the order of the mode of oscillation while the subscript j represents the order of the DFIG.

Thus, the objective function given by (33) comprises the sum of the PSS gains with a penalty because of phase compensation, subjected to the set of constrains given by Eqs. (34)–(36), which require, respectively, that damping should be higher than a given threshold, frequency should be within a given range and control variables should be within allowable physical limits.

The transfer function of the PSS expressed in terms of the control variables is given by [33]:

$$V_{PSS}(s) = K \frac{sT_W}{1 + sT_W} \left(\frac{1 + sT_n}{1 + sT_n/\alpha} \right)^N V_{in}(s), \tag{37}$$

where K is the PSS gain and T_W is the washout time constant.

The control variables that constitute the solution of the problem are, for each PSS, the gain, the number of lead-lag blocks N and the time constant values, $T_n = T_1$, and $\alpha = T_1/T_2$, of each of these blocks. Limits are also imposed to the gains of the stabilisers and to the time constants of the lead-lag blocks. The washout time constant is specified previously to the PSS design and it is not adjusted. The weighting factors w_{ji} are used to provide an indication of the best locations to install PSS. As the location is not a concern it was assumed that $w_{ji} = 1$.

Considering a number of operating scenarios nc, the PSS tuning problem is envisaged as multi-criteria minimization problem having nc attributes corresponding to the quality of the PSS performance in each scenario. A trade-off solution will be found in the non-dominated or Pareto-optimal border of the set of solutions in the attribute space. However, the recognition of this border is a difficult problem and several strategies may be adopted for this purpose. A simple one is the minimization of the weighted sum of the attributes, as

$$\min Q = \sum_{k=1}^{nc} z_k Q_k, \tag{38}$$

where z_k denotes the relative importance of scenario k.

This is equivalent of finding, over the Pareto border, the point closest to the ideal solution using the space metric L_1, although other metrics could be used.

Considering that all the scenarios have equal importance, all $z_k = 1$, the objective function given by Eq. (33) can be re-written as

$$\min Q = \min\{\max[Q_k]\} \tag{39}$$

The PSS control parameters derived from Eq. (39) corresponds to project the PSS with its worst behaviour as best as possible.

In order to obtain the PSS robust solution, an Evolutionary Particle Swarm Optimization (EPSO) tool was exploited. EPSO was built over the concepts of both evolutionary strategies and particle swarm optimization in an attempt to combine the best of both techniques [35] to handle a set of particles in order to find a suitable solution for PSS to install in DFIG. Each particle involves a set of parameters comprising both the strategic and the object parameters. The set of object parameters represents a potential robust solution for PSS. Thus, given a set of particles, for a given iteration, the general algorithm of EPSO can be described as follows [33]:

1. Replication of each particle r times;
2. Mutation of the strategic parameters of each particle;
3. Reproduction of the mutated particles by generating an offspring according to the particle movement rule;
4. Evaluation of the fitness of each particle by calculating the corresponding Q value;
5. Selection of the best particles, according to the criterion given by the objective function, to form the new generation.

It should be noted that each particle evaluation requires the calculation of the state matrix eigen-values and the further assessment of the modes of oscillation. On the other hand, the number of performed evaluations, N_1, grows linearly with the number of scenarios, as

$$N_1(nc) = r \times it \times p \times nc, \tag{40}$$

where r is the number of replications, it is the number of iterations, p is the number of particles and nc is the number of scenarios.

Since the number of operating scenarios is very high, a set of representative scenarios has to be identified before running this proposed PSS tuning procedure. Thus, the following section proposes a suitable procedure for identification of representative operating scenarios.

5.3 *Identification of Representative Operating Scenarios*

The integration of wind power increases largely the diversity of system operating conditions and, thereby, the resulting number of operating scenarios. Moreover, the effectiveness of the PSS to install in the DFIG depends on the amount of wind

generation as a result of variations of the number of wind turbines in operation and of the wind speed variability. These factors make the identification of a reduced set of relevant scenarios a very hard task.

The operating scenarios can be generated automatically using a structured Monte Carlo procedure. However, the large number of operating scenarios to be generated will lead to a computational burden that may render unfeasible the proposed PSS robust tuning procedure. Therefore, in a second phase, the set of all possible operating scenarios has to be reduced to a much smaller number of scenarios representing the most unfavourable operating conditions, the so-called set of worst case scenarios. Thus, a suitable solution derived from this set of scenarios will be acceptable for all the operating scenarios.

In order to select the set of worst case scenarios, some engineering judgment is required taking advantage of the well known fact that transmission of bulk power through weak transmission lines tends to originate low damped modes of oscillation. This is, however, a trial and error approach that can be tedious when the number of scenarios is very high.

To speed up the identification of the worst case scenarios without ignoring operating conditions that will be less obvious but relevant for PSS tuning, a heuristic approach should be followed, as proposed in [33]. Two different sets are created. The set A will include all the scenarios while the set B will be empty and eventually will contain some of the worst scenarios. Then, the next steps are followed:

1. Calculate the fitness for each scenario according with the Eq. (33);
2. Select the scenario with worst performance corresponding to the highest values of the fitness;
3. Include the selected scenario in set B if it is not a member of this set. Otherwise the solution was found and the algorithm stops;
4. Identify the PSS robust solution by tuning simultaneously all PSS using the operating scenarios grouped in set B;
5. Evaluate the robust solution considering all the operating scenarios;
6. If the worst fitness is better than a given limit, previously specified, the solution was found and the algorithm stops. Otherwise check the number of iterations;
7. Stop the algorithm if the number of iterations exceeds its maximum value. Otherwise return to step 1.

The result of this algorithm will be a robust solution for the PSS tuning problem, that is, a suitable solution for all operating scenarios grouped in set B. However, if the algorithm stops in step 6, because the maximum number of iterations was achieved, it is not assured that a robust solution was found. Nevertheless, that solution should lead to a reasonable damping improvement. In both cases the number of performed evaluations by the proposed heuristic is given by:

$$N_2(a) = \sum_{i=1}^{a} N_1(i) + nc(a+1), \tag{41}$$

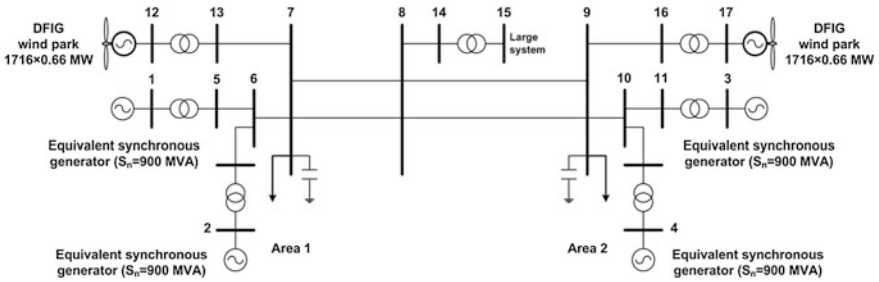

Fig. 20 Single line diagram of the test system

where N_2 is the total number of evaluations and a is the number of iterations performed by the heuristic and corresponds to the number of scenarios in set B.

Equation (41) comprises two components: the number of evaluations required to tune the PSS parameters using the operating scenarios in the set B and the number of evaluations performed to assess the adequacy of the robust solution regarding the scenarios of the set A. It should be noted that the first component has a much larger weight in the total number of the performed evaluations.

5.4 The Test System

The performance of the algorithm presented in Sect. 5.2 was evaluated using the test system depicted in Fig. 20, comprising two areas connected to a large system. Each area contains two synchronous equivalent generators, one wind park equipped with DFIG and represented through an equivalent machine, an equivalent load and a capacitor bank. The generator connected to bus 15 corresponds to the large system represented as an infinite bus.

The synchronous generators represent a group of strongly coupled generators. The equivalent model consists of a six-order model, neglecting the magnetic saturation, together with voltage regulators represented by the IEEE type 1 model [26]. The DFIG with PSS are represented by the model presented in Sect. 5.1. Loads and capacitor batteries are modelled as constant impedances.

5.5 Generation of the Operating Scenarios

The scenarios to be considered are generated by the automatic procedure presented in Sect. 5.2, taking into account several issues with a significant influence on the damping levels. Then, variation levels with respect to the reference values defined for the base case [32] were considered as follows:

1. Unit commitment of synchronous generators and wind farms. Generators connected to buses 1 and 2 are out of service to accommodate wind generation while generators connected to buses 3 and 4 are kept in operation. Regarding wind generation, it was also considered that both wind farms can be out of operation, one half of the DFIG are in operation and all the DFIG are in operation.
2. Load level. A variation of 25 % around the reference value was considered.
3. Generation of synchronous machines. A variation of 25 % around the reference value was also considered.
4. Wind speed corresponding to different values of active power. Variations in the range between 7 and 10 m/s for the wind park connected to bus 12 and variations in the range between 8 and 14 m/s for the wind farm connected to bus 17 were considered.
5. Grid configuration. It was considered that one of the lines between buses 7 and 8 is switched off and one of the lines between buses 8 and 9 is switched off.

In order to generate the operating scenarios the following procedure was then adopted:

1. The operating conditions of the base scenario were changed according to the defined ranges forming a combined set of operating scenarios. Thus, starting from the base scenario, the unit commitment was changed and the resulting scenarios were stored. Then, the loads of all the stored scenarios were changed generating, thus, new scenarios that were also stored. In the same way, the active power of synchronous generators as well as the wind speed and the grid configuration were modified.
2. A power flow was performed for all the operating scenarios in order to eliminate unfeasible scenarios.
3. The modes of oscillation for all the feasible scenarios were calculated and analysed.

This procedure generated a set of 1,300 operating scenarios requiring, thus, further selection. The heuristic approach presented before was used for selecting the worst case scenarios. In these scenarios the global level of wind generation reaches 50 % in some cases, being the wind power generation in area 1 around 70 %, whereas in area 2 it is approximately 45 %.

5.6 Results and Discussion

The electromechanical modes of oscillation for these scenarios are presented in Fig. 21a, showing that the minimum damping of each scenario varies between 5 and 18 %. The low damping is mainly due to a mode associated with the synchronous generator connected to bus 2.

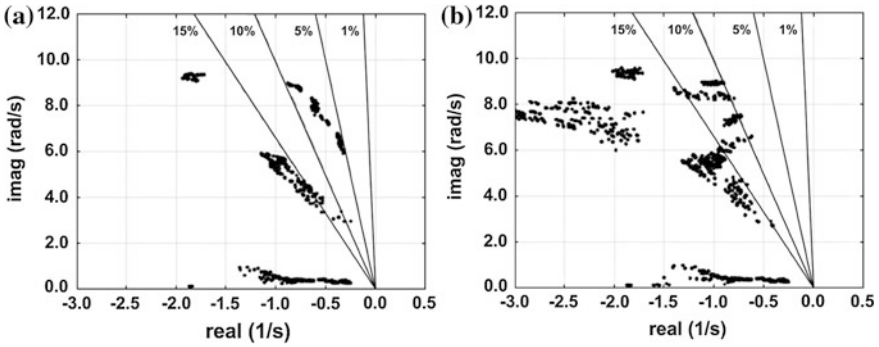

Fig. 21 Pole map: (**a**) without PSS installed in DFIG; (**b**) with PSS installed in DFIG

Table 3 Characterisation of the operating conditions for the worst case scenarios

nc	P_L (MW)	P_{G12} (MW)	P_{G2} (MW)	P_{G3} (MW)	F_{7-8} (MW)	F_{8-9} (MW)
1	2334.0	358.6	525.0	593.3	113.7	−594.5
2	2917.5	240.2	700.0	593.3	−23.4	395.1
3	2334.0	240.2	350.0	593.3	−178.1	−594.5
4	2917.5	240.2	525.0	719.1	−196.4	−388.3
5	2917.5	700.3	700.0	719.1	1109.7	581.1

PSS installed in synchronous generators connected to buses 1 and 3 are considered to be in operation. However, as these PSS were tuned for scenarios without wind generation, the damping level is not adequate since many modes of oscillation exhibit damping levels lower than 10 and 15 %. Another reason for the low damping levels is related with the fact that one synchronous generator equipped with PSS was out of service in order to accommodate the surplus of wind generation in the system.

PSS to install in DFIG connected to buses 12 and 17 were tuned using the algorithm presented in Sect. 5.2 in order to find a robust solution able to increase damping in all modes of oscillation to levels above 15 % with frequency variations less than 5 % for all the operating scenarios. The selected worst case scenarios are characterised in Table 3, through the system total load, production of generators connected to buses 2 and 12 and the active power flow through the interconnection lines. The damping and frequency of the less damped modes of oscillation with and without PSS installed in DFIG are also presented in Table 4.

With the PSS tuning algorithm, a robust solution was found with less than 160,000 evaluations considering 2 replications of each particle ($r = 2$), a constant number of particles ($p = 20$) and the number of iterations was defined to be $it = 250$. The obtained PSS parameters are presented in Table 5, where de generator number corresponds to the number of the connecting bus.

The modes of oscillation for all the scenarios can be observed from Fig. 21b.

Table 4 Characterisation of the modes of oscillation for the worst case scenarios

Without PSS in DFIG				With PSS in DFIG		
c	ς (%)	f(Hz)	Gen.	ς (%)	f(Hz)	Gen.
1	7.23	1.19	2	10.20	1.19	2
2	5.59	1.03	2	13.24	0.99	2
3	8.39	0.47	3	10.24	1.43	2
4	5.59	1.08	2	9.31	1.05	2
5	10.10	0.54	1	14.53	0.46	1

Table 5 Value of the PSS parameters

Gen.	K	N	T	α
1	6.06	2	0.5155	27.28
3	7.72	2	0.4716	21.83
12	0.12	0	–	–
17	0.95	2	0.9968	0.27

The obtained solution is able to increase the damping levels for more adequate values. However, the target value of 15 % was not achieved for all the modes of oscillation, since it is not possible to obtain a better solution for scenario 4 without reducing the damping levels of the other scenarios as a result of the fact that DFIG do not participate in electromechanical oscillations thereby contributing only indirectly to increase the damping levels. On the other hand, the selected operating scenarios represent extremely unfavourable operating conditions for PSS.

Finally, the PSS performance was also assessed through non-linear time domain simulations using the PSS/E dynamic simulation tool, considering a step change with amplitude of 0.01 p.u. applied to the reference voltage of the AVR associated to generator 2 (Fig. 22) and, in a second simulation example (Fig. 23), the occurrence of a three-phase short circuit, taking place at bus 8, with duration of 150 ms. Because the number of scenarios is high, results for one case are presented next in order to illustrate the system response. It should be noted that the generator number corresponds to the bus number. Also, the active power output is referred to the system base, $S_b = 100$ MVA.

As it can be observed from Figs. 22 and 23, the installation of PSS in DFIG tuned with the proposed approach lead to quite adequate results. The damping improvement is clearly observed in synchronous generator connected to bus 2 (Generator 2) and also in the power flow through the line between buses 7 and 8.

The results obtained allow concluding that although not participating in the electromechanical oscillations, DFIG can contribute effectively to provide additional damping. However, the integration of wind generation increases the system operation complexity, thereby increasing the difficulty to perform PSS tuning. Under these circumstances, the heuristic based approach used to select the representative set of operating scenarios plays a key role regarding the reduction of the computational burden of PSS robust tuning. Using the representative set of

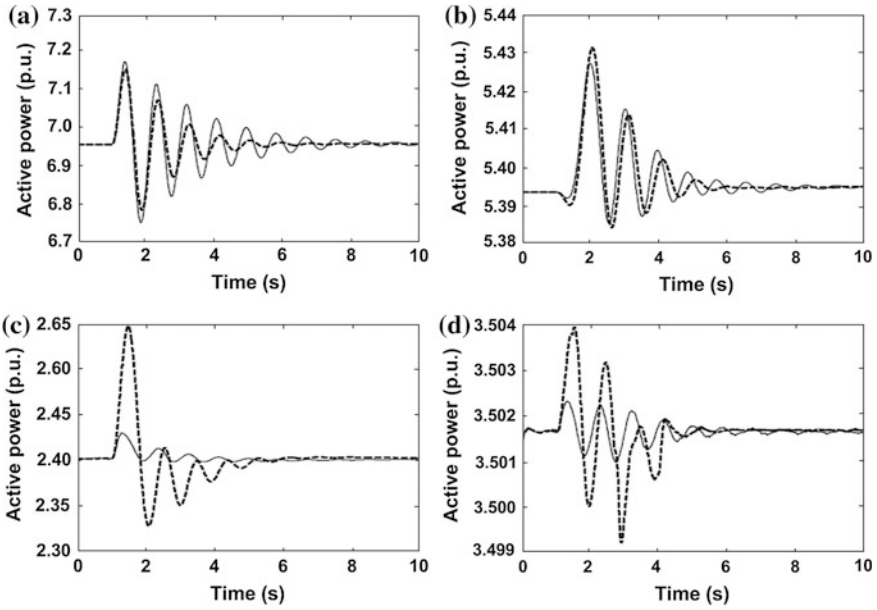

Fig. 22 Response to a step change in reference voltage of generator 2 without PSS installed in DFIG (*full line*) and with PSS installed in DFIG (*dashed line*): (**a**) active power output of generator 2; (**b**) active power output of generator 3; (**c**) active power output of generator 12; (**d**) active power output of generator 17

scenarios corresponding to the worst operating conditions, the best solution found by the EPSO based approach correspond to the robust solution for PSS.

6 External FRT Solutions Used in Wind Parks Equipped with FSIG

The STATCOM based solution connected to wind farm terminals is adopted to provide FRT capability of wind farms equipped with FSIG. For this purpose this static compensator device is controlled to regulate the wind farm terminal bus voltage through the reactive power injection into the grid. Thus, when system voltage drops following a grid disturbance, the STATCOM injects immediately reactive power in an attempt to limit the voltage dip. In this section, the commonly used control functions are presented and the STATCOM performance is evaluated through numerical simulations considering the occurrence of both balanced and unbalanced faults taking place in the utility ac grid.

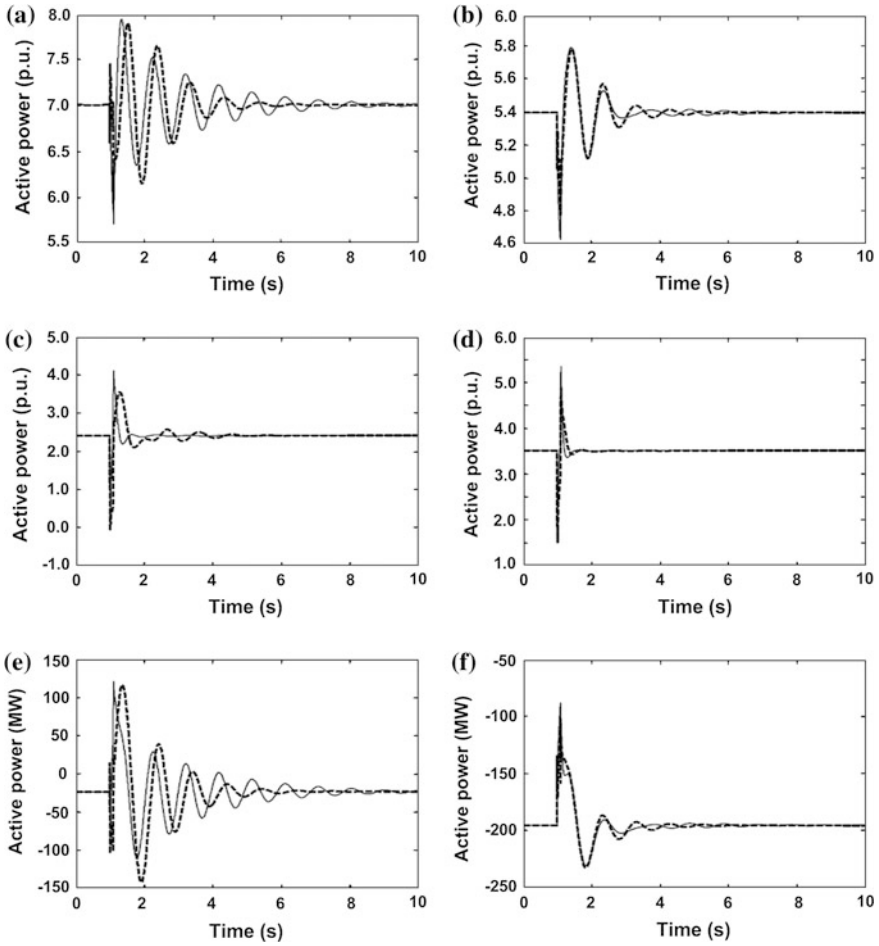

Fig. 23 Response to a 150 ms short circuit in bus 8, without PSS installed in DFIG (*full line*) and with PSS installed in DFIG (*dashed line*): (**a**) active power output of generator 2; (**b**) active power output of generator 3; (**c**) active power output of generator 12; (**d**) active power output of generator 17; (**e**) active power flow in line 7–6; (**f**) active power flow in line 9–8

6.1 The STATCOM Control System

The STATCOM consists of a three-phase Voltage Source Converter (VSC) shunt connected to the wind farm terminal bus through a coupling transformer [21], as it can be observed from Fig. 24.

The VSC using IGBT based PWM inverter uses a PWM technique to synthesize a sinusoidal waveform from the dc voltage source corresponding to voltage at the dc link. Power electronic components are switched on and off at high frequency (several kHz) and, therefore, high frequency harmonics and ripples will be limited

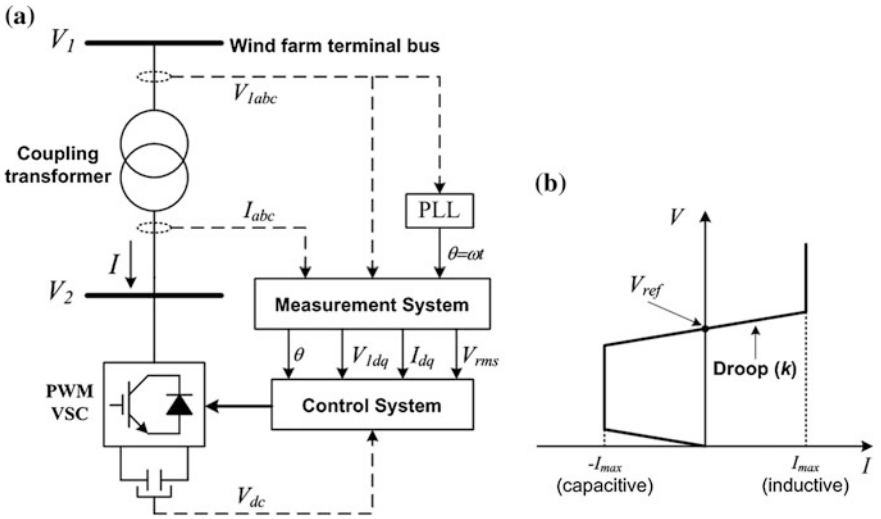

Fig. 24 The STATCOM: (**a**) structure; (**b**) *V–I* characteristic

by connecting filters at the ac side of the VSC [10]. As a consequence of the high switching frequency, a small time step would be required for time domain simulations. Since the VSC behaviour is not a matter of concern in this research, a simplified modelling approach was adopted, such that the VSC reproduces an ideal the reference voltage provided from the control system.

According to Fig. 24a, the active and reactive power transfer, P and Q, respectively, between the VSC and the grid can be expressed as follows:

$$\begin{cases} P = \frac{V_1 V_2 \sin\delta}{X} \\ Q = \frac{V_1(V_1 - V_2\cos\delta)}{X} \end{cases}, \tag{42}$$

where X is the reactance of both the interconnection transformer and the VSC filter and δ is the angle of V_1 with respect to V_2.

In steady state operation $\delta = 0$ and only reactive power is flowing. The VSC absorbs reactive power if V_2 is lower than V_1. Otherwise it generates reactive power.

As the VSC is controlled to regulate V_1, it implements the *V–I* characteristic presented on Fig. 24b. Thus, the STATCOM can operate with its rated current even at reduced voltages and, in addition, as long as the reactive current stays within its minimum and maximum values imposed by the converter rating, $-I_{\max}$ and $I_{\max}$, respectively, the voltage is regulated according to its reference value, V_{ref}. However, a voltage droop (usually between 1 and 5 % at maximum reactive power output) is normally used, being the *V–I* characteristic described by

$$V = V_{ref} + k \times I, \tag{43}$$

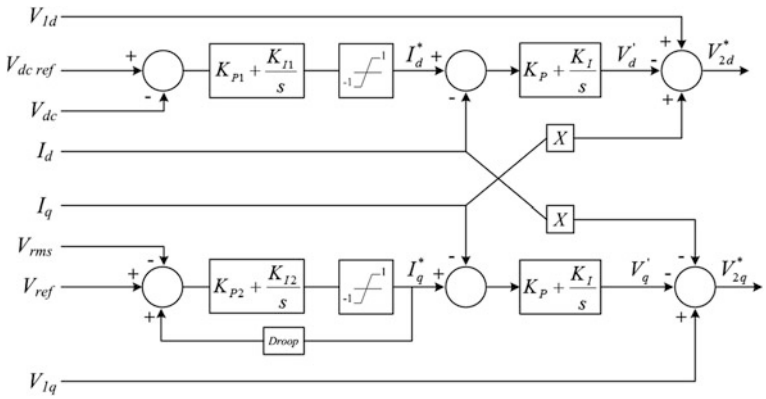

Fig. 25 The VSC control scheme

where V is the positive sequence voltage (p.u.), I is the reactive current (p.u./P_{nom}) and P_{nom} is the three-phase nominal power of the STATCOM.

The VSC control system is designed based on the vector control technique, which has been commonly used to deal with fast dynamic requirements and to provide decoupling control ability [10, 16, 19, 36, 43, 45, 49]. Thus, using the d–q reference frame rotating at the grid frequency, ω, with the q-axis 90° ahead the d-axis, being the d-axis aligned with the position of the wind farm terminal bus voltage, the active and reactive power can be controlled independently using I_d and I_q, respectively, so that the reactive power flow can be controlled via I_q whereas the dc-link voltage can be controlled via I_d [10]. In order to synchronize on the positive sequence component of the three-phase terminal voltage V_1, and to provide the angle $\theta = \omega t$ to the Park transformation [26] as well as to its inverse, a Phase Looked Loop (PLL) is employed, as it can be observed from Fig. 24.

The VSC control scheme comprises two control loops based on PI controllers, as illustrated in Fig. 25. The first control loop is responsible for keeping constant the dc-link voltage through a small active power exchange with the ac network in order to compensate the active power losses regarding both the transformer and the inverter. The second control loop controls the terminal voltage through the reactive power exchange with the ac network.

For these purposes, the PI controllers involve a cascade structure, as it can be observed from Fig. 25. The outer side PI controllers are used to regulate the dc-link voltage V_{dc}, and the magnitude of the direct component of the terminal voltage V_{rms}, providing thus active and reactive current references, respectively, I_d^* and I_q^*. These current references are limited between 1 p.u. capacitive and −1 p.u. inductive. The PI2 controller has a droop characteristic to allow some variations around the terminal voltage, according to Eq. (43). The inner side PI controllers are used to regulate the active and reactive currents (I_d and I_q) by providing

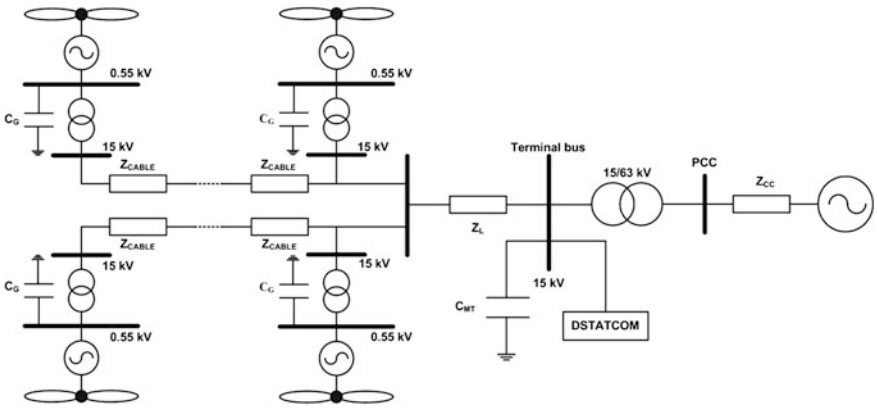

Fig. 26 The test system single line diagram

voltage references V_{2d}^* and V_{2q}^*, respectively, which, after a *dq*-to-*abc* transformation, are sent to the PWM signal generator of the VSC in order to control the magnitude and the phase of the terminal voltage V_2.

6.2 The Test System

The test system presented in Fig. 26 was used to evaluate the STATCOM performance regarding FRT capability wind farms equipped with FSIG when facing external faults using an *EMTP–RV*® dynamic simulation tool.

This test system is a 10 MW wind farm connected to the utility system. The wind farm comprises 20 SCIG with a rating of 500 kW. Each wind turbine is connected to the wind farm internal network of 15 kV through a 630 kW, 0.55/15 kV transformer. Low Voltage (LV) capacitor batteries for individual SCIG reactive power compensation are connected to its terminal bus in order to assure the reactive power requirements under unload conditions. Another capacitor bank connected on the Medium Voltage (MV) side of the wind farm substation is used to provide the additional reactive power required by the SCIG when operated under load conditions and reactive power must be injected into the ac network under normal operating conditions in order to comply with a given power factor requested by system operators. In order to provide FRT capability, this wind farm is also equipped with a STATCOM with 10 MVA of rating power. The wind farm is connected to the High Voltage (HV) network by means of a 10 MVA, 15/63 kV transformer. The short-circuit power at PCC is 200 MVA.

The STATCOM model was built under *EMTP-RV*® environment (version 1.0.2), since it is not available in this version library. The induction machine model is based on a fourth-order state space model [52] built in the library in *EMTP-RV*®.

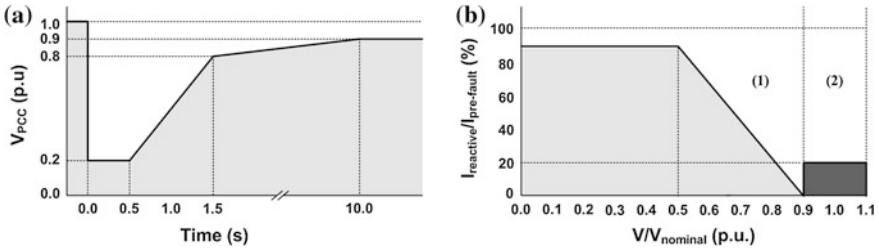

Fig. 27 Characteristic curves of Portuguese grid codes: (**a**) time–voltage characteristic; (**b**) characteristic curve of reactive current delivered by wind farms during/after voltage dips *1* fault and recovery region; *2* normal operation region

The wind speed is reproduced through the mechanical torque which is applied to the induction generator model. The utility system is represented by a constant voltage source connected in series with the corresponding equivalent impedance of Thevenin. The remaining components are represented through the models available on *EMTP-RV*® library.

6.3 Simulation Results and Discussion

The FRT capability of wind farms equipped with FSIG was evaluated considering the Portuguese proposal of grid codes for wind farms connection [16]. Regarding FRT requirements, wind power plants must fulfil the following minimum technical requirements:

- To remain in operation during voltage dips, if the wind farm terminal bus voltage remains above the curve depicted in Fig. 27a during the fault and after its clearance for the time limits also defined according to Fig. 27a;
- To deliver reactive power during voltage dips in order to provide voltage support for the network. The requested reactive power is indexed to the reactive current flowing through PCC before the fault occurrence, being the wind farm obliged to stay in the white region of the curve depicted in Fig. 27b.

In order to demonstrate the STATCOM contribution to provide FRT capability of wind farms equipped with FSIG, the most severe fault conditions regarding voltage recovery were considered. Thus it was assumed that the test system wind farm is operated with a $tg(\phi) = 0.2$, near its rated power, corresponding to the maximum amount of reactive power drawn to SCIG. Then, a three-phase short-circuit is simulated on the ac network, far from the wind farm, at $t = 1$ s and with a clearance time of 500 ms. The voltages at the PCC and at the wind farm terminal bus are depicted in Fig. 28 when the wind farm is operated with and without the STATCOM.

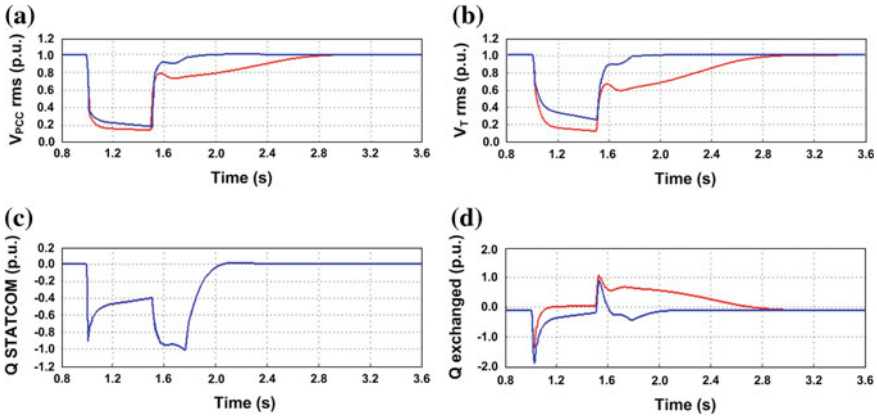

Fig. 28 System dynamic behaviour following a balanced fault: (**a**) voltage at the PCC with STATCOM (*blue*) and without STATCOM (*red*); (**b**) terminal bus voltage with STATCOM (*blue*) and without STATCOM (*red*); (**c**) reactive power injected from the STATCOM; (**d**) reactive power exchange to the ac grid with STATCOM (*blue*) and without STATCOM (*red*)

Without the STATCOM, the voltage at the PCC drops below 0.2 p.u. during the fault, leading with the wind farm disconnection according to the considered FRT requirements. The STATCOM based solution avoids this situation, since the voltage at the PCC remains above 0.2 p.u., as it can be observed from Fig. 28a, contributing thus to FRT enhancement. In addition, after the fault is cleared, the voltage recovers faster and within the time limits required by the FRT requirements. Moreover, a better improvement is achieved regarding the terminal bus voltage by means of reactive power injection into the grid from the STATCOM during the fault and after its clearance, as it can be observed from Fig. 28b.

The STATCOM control system reacts immediately to a sudden voltage dip, saturating the controller and injecting the maximum reactive current into the grid, as illustrated in Fig. 28c. However, it should be noted that the reactive power injection is limited by the voltage drop and therefore the STATCOM provides a little contribution for voltage support during the fault. In contrast, after the fault is cleared, the reactive power injected from the STATCOM corresponds to its rated power contributing to a faster voltage recovery and a clear increase of the system stability margin. In addition, the magnetization process of FSIG is dynamically supported making it possible to decrease the rotor speed and to reduce the reactive power consumption from the grid, as it can be observed from Fig. 28d.

When the STATCOM is used to perform voltage control, since the VSC control system is based on the ac-positive sequence voltage measured at the STATCOM connection point, the same amount of reactive power is injected on the three-phases. The results obtained from numerical simulation demonstrate the effectiveness of this commonly used control technique under balanced conditions, such as following three-phase short-circuits, in which the voltages on the three phases experiment similar amplitudes of voltage drop.

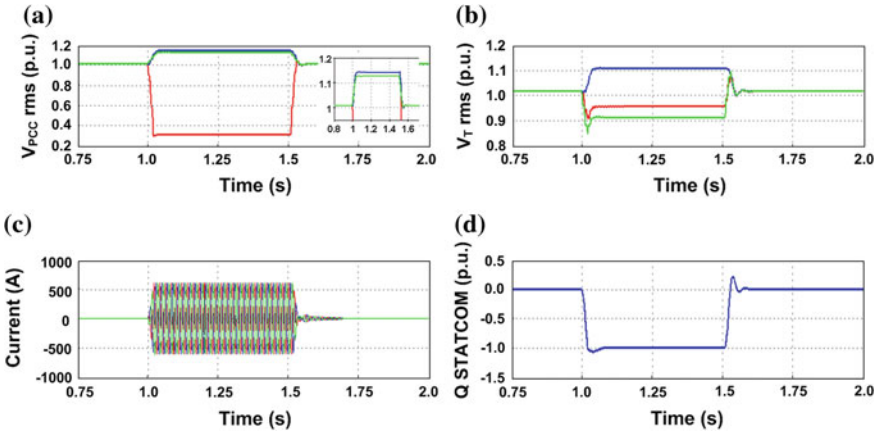

Fig. 29 System dynamic behaviour following an unbalanced fault: (**a**) voltage at the PCC—phase a (*red*), phase b (*blue*) and phase c (*green*); (**b**) terminal bus voltage—phase a (*red*), phase b (*blue*) and phase c (*green*); (**c**) STATCOM reactive current—phase a (*red*), phase b (*blue*) and phase c (*green*); (**d**) reactive power injected from the STATCOM

Although the balanced faults are the most severe ones, its occurrence is extremely rare. In contrast, unbalanced faults, which occur when one or two phases are shorted to ground or to each other, happen most often leading with negative sequence components in the ac grid voltages. Thus, the STATCOM dynamic performance to provide FRT of wind farms equipped with FSIG should also be evaluated when facing unbalanced faults. For this purpose, a single phase short-circuit taking place on phase *a* was simulated on the HV network at $t = 1$ s and with a clearance time of 500 ms, considering that all the SCIG are operated near one half of their ratings and the MV capacitor battery assures the wind farm operation with $tg(\varphi) = 0.4$ in order to comply with power factor requirements. The results obtained are presented in Fig. 29.

The 15/63 kV transformer of type ΔY influences on how the grid fault appears on the wind farm terminal bus, as it can be observed from Fig. 29a, b. Although only the phase *a* was short to ground, both phases *a* and *c* experimented voltage dips, even with a much reduced magnitudes. However, the STATCOM injects a balanced three-phase reactive current into the ac grid, as it can be observed from Fig. 29c, leading with considerable over voltages experimented by the non-faulted phases, as it can be observed from Fig. 29a, b. In fact, the voltage at the PCC, regarding phase *b* and phase *c*, experiments over voltages above 1.1 p.u. and a similar situation is verified regarding the wind farm terminal bus voltage on phase *c*. After the fault elimination, transient over voltages take place on phase *a* and phase *b* of the wind farm connection point, as it can be observed from Fig. 29a. It should also be noted that the behaviour of the ac-positive sequence of the terminal bus voltage allows the STATCOM to inject its maximum reactive current, according to the *V–I* characteristic depicted in Fig. 24b, and therefore the reactive

power output corresponds to its rated power. In contrast with the three-phase short-circuit simulated previously, the terminal bus voltage drop is much reduced allowing the maximum reactive power injection into the ac grid, as it can be observed from Fig. 29d.

The results obtained demonstrate that the STATCOM provides voltage support during voltage dips that arise following the occurrence of external short circuits, reducing thus the voltage drops, and contributes to fast voltage recovery after the fault clearing. Therefore, the STATCOM can be considered as an effective mean to improve FRT capability of existing wind farms equipped with FSIG. However, in case of unbalanced faults, such as a single-phase short circuit, over voltages can arise on the non-faulted phases, which can trigger the over voltage protections and subsequent wind farm disconnection, missing the FRT capability improvement. In order to avoid such situations, complementary control procedures to define the amount of reactive power injection should be derived. For this purpose, negative sequence of the voltage at the STATCOM connection point should also be taken into account. On the other hand, when possible, an adjustment of the settings of the over voltage protections should be performed.

7 Final Remarks

An effective integration of large scale wind generation leads to a new challenge clearly stated as control wind power in a similar way to conventional power plants equipped with synchronous generators. Therefore, the stability of fundamental electric parameters, frequency and voltage, has to be assured. Active power control is required for frequency regulation and reactive power control is required for voltage regulation. In addition, wind parks should comply with FRT requirements, according to the grid codes imposed by transmission system operators.

For this purpose, the variable speed feature of WTGS plays a key role. Regarding DFIG, advanced control functionalities have been developed aiming to improve the DFIG performance regarding the compliance with grid code requirements, such as FRT capability and primary frequency control. The main focus is put on the RSC, since it responsible for the generator operation and control in terms of speed and independent control of active and reactive power outputs. Also, classical PSS should be included on the RSC control system allowing DFIG equipped with PSS to provide damping contributions, enhancing thus the system small signal stability in case of conventional generation with PSS installed be replaced by wind based generation.

Wind farms equipped with FSIG require the adoption of external solutions to provide FRT capability. Although STATCOM based solutions are an effective mean for this purpose, the need of including complementary control procedures based on the negative sequence of the voltage at the STATCOM connection point should be evaluated when facing unbalanced faults in order to prevent the occurrence of over voltages in the non-faulted phases.

Discussion of advanced control functionalities to be implemented in control systems of power electronic converters of variable speed WTGS and STATCOM together with dynamic modelling issues will represent new insights for evaluating the power system robustness of operation following the increasing integration levels of wind based generation.

Acknowledgments The authors would like to acknowledge to FCT, Fundação para a Ciência e Tecnologia (Portuguese Foundation for Science and Technology), by its support within the Grants SFRH/BD/18469/2004 and SFRH/BPD/64022/2009.

References

1. Achmatov V (2002) Variable speed wind turbines with doubly fed induction generators. Part IV: Uninterrupted operation features at grid faults with converter control coordination. Wind Eng 27:519–529
2. Akhmatov V (2003) Analysis of dynamic behaviour of electric power systems with large amount of wind power. PhD Thesis, Technical university of Denmark, ISBN 87-91184-18-5
3. Akagi H, Kanazawa Y, Nabae A (1984) Instantaneous reactive power compensators comprising switching devices without energy storage components. IEEE Trans Ind Appl (IA-20):625–630
4. Almeida RG, Castronuovo E, Peças Lopes JA (2006) Optimum generation control in wind parks when carrying out system operator requests. IEEE Trans Power Syst 21:718–725
5. Almeida RG, Lopes JA (2005) Primary frequency control participation provided by doubly fed induction wind generators. In: Proceedings of 15th power systems computation conference, pp 1–7
6. Almeida RG, Peças Lopes JA (2007) Participation of doubly fed induction wind generators in system frequency regulation. IEEE Trans Power Syst 22:944–950
7. Almeida RG, Lopes JP, Barreiros JAL (2004) Improving power system dynamic behaviour through doubly fed induction machines controlled by static converter using fuzzy control. IEEE Trans Power Syst 19:1942–1950
8. Aten M, Martinez J, Cartwright PJ (2005) Fault recovery of a wind farm with fixed-speed induction generators using a STATCOM. Wind Eng 29:365–375
9. Barbosa P, Rolim L, Watanabe E, Hanitsch R (1998) Control strategy for grid connected DC–AC converters with load power factor correction. In: IEE proceedings of generation, transmission and distribution, vol 145, pp 487–491
10. Chen Z, Hu Y, Blaabjerg F (2007) Stability improvement of induction generator-based wind turbine systems. IET Renew Power Gener 1:81–93
11. Do Bomfim A, Taranto G, Falcão D (2000) Simultaneous tuning of power system damping controllers using genetic algorithms. IEEE Trans Power Syst 15:163–169
12. Ekanayake J, Holdsworth L, Jenkins N (2003) Control of DFIG wind turbines. Power Eng J 17:28–32
13. Ekanayake JB, Holdsworth L, XueGuang W et al (2003) Dynamic modeling of doubly fed induction generator wind turbines. IEEE Trans Power Syst 18:803–809
14. Ekanayake J, Jenkins N (2004) Comparison of the response of doubly fed and fixed speed induction generator wind turbines to changes in network frequency. IEEE Trans Energy Convers 19:800–802
15. Erlich I, Wrede H, Feltes C (2007) Dynamic behaviour of DFIG-based wind turbines during grid faults. In: Proceedings of power conversion conference 2007, vol 1, pp 1195-1200

16. Estanqueiro A, Castro R, Flores P, Ricardo J, Pinto M, Rogrigues R, Peças Lopes JA (2007) How to prepare a power system for 15% wind energy penetration: The Portuguese case study. Wind Energy 11:75–84
17. Feijoo A, Cidras J, Carrillo C (2000) A third order model for the doubly-fed induction machine. Elect Power Syst Res 56:121–127
18. Feltes C, Engelhardt S, Kretschmann J, Fortmann J, Koch F, Erlich I (2009) Comparison of the grid support capability of DFIG-based wind farms and conventional power plants with synchronous generators. In; Proceedings of IEEE power and energy society general meeting 2009, vol 1, pp 1–7
19. Gaztañaga H, Etxeberria-Otadui I, Ocnasu D, Bacha S (2007) Real-time analysis of the transient response improvement of fixed-speed wind farms by using a reduced-scale STATCOM prototype. IEEE Trans Power Syst 22:658–666
20. Hansen A, Sorensen P, Iov F, Blaabjerg F (2006) Centralized power control of wind farm with doubly fed induction generators. Renew Energy 31:935–951
21. Hingorani NG, Gyugyi L (2000) Understanding FACTS: concepts and technology of flexible AC transmission systems. Wiley-IEEE Press, Hardcover
22. Holdsworth L, Ekanayake J, Jenkins N (2004) Power system frequency response from fixed speed and doubly fed induction generators-based wind turbines. Wind Energy 7:21–35
23. Hughes F, Anaya-Lara O, Jenkins N, Strbac G (2005) Control of DFIG-based wind generation for power network support. IEEE Trans Power Syst 20:1958–1966
24. Hughes F, Anaya-Lara O, Jenkins N, Strbac G (2006) A power system stabilizer for DFIG-based wind generation. IEEE Trans Power Syst 21:763–772
25. Koch F, Erlich I, Shewarega F (2003) Dynamic simulation of large wind farms integrated in a multimachine network. In: Proceedings of IEEE power engineering society general meeting, vol 1, pp 2159–2164
26. Kundur P (1994) Power system stability and control. McGraw-Hill, New York
27. Lee C (1990) Fuzzy logic in control systems: fuzzy logic controllers. IEEE Trans Syst Man Cybern 20:404–418
28. Lei Y, Mullane A, Lightbody G, Yakamini R (2006) Modeling of the wind turbine with a doubly fed induction generator for grid integration studies. IEEE Trans Energy Convers 21:257–264
29. Li H, Chen Z (2008) Overview of different wind generation systems and their comparisons. IET Renew Power Gener 2:123–138
30. Li H, Philip C, Huang H (2001) Fuzzy neural intelligent system. CRC Press, New York
31. Machmoum M, Poitiers F, Darengosse C, Queric A (2002) Dynamic performance of a doubly-fed induction machine for a variable-speed wind energy generation. In: Proceedings of international conference on power systems technology 2002, vol 4, pp 2431–2436
32. Mendonça A, Peças Lopes J A (2003) Robust tuning of PSS in power systems with different operating conditions. In: Proceedings of IEEE bologna power tech conference, vol 1, pp 1–7
33. Mendonça A, Peças Lopes JA (2009) Robust tuning of power system stabilisers to install in wind energy conversion systems. IET Renew Power Gener 3:465–475
34. Michalke G, Hansen AD (2010) Modelling and control of variable speed wind turbines for power system studies. Wind Energy 13:307–322
35. Miranda V (2005) Evolutionary algorithms with particle swarm movements. In: Proceedings of 13th international conference on intelligent systems applications to power systems, vol 1, pp 6–21
36. Molinas M, Suul JA, Undeland T (2007) Improved grid interface of induction generators for renewable energy by use of STATCOM. In: Proceedings of ICCEP'07, vol 1, pp 215–222
37. Morren J, Haan S, Kling W, Ferreira J (2006) Wind turbines emulating inertia and supporting primary frequency control. IEEE Trans Power Syst 21:433–434
38. Novotny DW, Lipo TA (2000) Vector control and dynamics of AC drives. Oxford University Press, New York

39. Nunes M, Bezerra U, Peças Lopes JA, Zurn H, Almeida RG (2004) Influence of the variable speed wind generators in transient stability margin of the conventional generators integrated in electrical grids. IEEE Trans Energy Convers 9:692–701
40. Pena R, Clare JC, Asher GM (1996) Doubly fed induction generator using back-to-back PWM converters and its application to variable-speed wind energy generation. In: IEE proceedings of electric power applications, vol 143, pp 231–241
41. Poller MA (2003) Doubly-fed induction machine models for stability assessment of wind farms. In: Proceedings of 2003 IEEE bologna power tech conference, vol 3, pp 1–6
42. Pourbeik P, Gibbard M (1998) Simultaneous coordination of power systems stabilizers and FACTS devices stabilizers in a multimachine power system for enhancing dynamic performance. IEEE Trans Power Syst 13:473–479
43. Qi L, Langston J, Steurer M (2008) Applying a STATCOM for stability improvement to an existing wind farm with fixed-speed induction generators. IEEE power and energy society general meeting—conversion and delivery of electrical energy in the 21st century, vol 1, pp 1–6
44. Qiao W, Zhou W, Aller JM, Harley RG (2008) Wind speed estimation based sensorless output maximization control for a wind turbine driving a DFIG. IEEE Trans Power Electron 23:1156–1169
45. Rao P, Crow ML, Yang Z (2000) STATCOM control for power system voltage control applications. IEEE Trans Power Delivery 15:1311–1317
46. Resende FO, Peças Lopes JA (2009) Evaluating the performance of external fault ride through solutions used in wind farms with fixed speed induction generators when facing unbalanced faults. In: Proceedings of the IEEE bucharest power tech 2009, vol 1, pp 1–6
47. Rodriguez J et al (2002) Incidence of power system dynamics of high penetration of fixed speed and doubly fed wind energy systems: study of the Spanish case. IEEE Trans Power Syst 19:1089–1095
48. Rogers GJ (2000) Power system oscillations. Kluwer Academic Publishers, Boston
49. Rogers GJ, Shirmohammadi D (1987) Induction machine modelling for electromagnetic transient program. IEEE Trans Energy Convers (EC-2):622–628
50. Salman SK, Teo ALJ (2003) Windmill modelling considerations and factor influencing the stability of grid connected wind power based embedded generator. IEEE Trans Power Syst 18:793–802
51. Slootweg JG, Haan SWH, Polinder H, Kling L (2003) General models for representing variable speed wind turbines in power system dynamics simulations. IEEE Trans Power Syst 18:144–151
52. Stavrakakis G, Kariniotakis G (1995) A general simulation algorithm for the accurate assessment of isolated diesel-wind turbines systems interaction—part I: a general multimachine power system model. IEEE Trans Energy Convers 10:577–583
53. Stavrakakis G, Kariniotakis G (1995) A general simulation algorithm for the accurate assessment of isolated diesel-wind turbines systems interaction—part II: implementation of algorithm and case studies with induction generators. IEEE Trans Energy Convers 10:584–590
54. Tsili M, Papathanassiou S (2009) A review of grid code technical requirements for wind farms. IET Renew Power Gener 3:308–332